AD_____

Award Number: DAMD17-03-1-0480

TITLE: Theoretical Modeling of Molecular Mechanisms, Strains, and Time Scales in Prion Diseases

PRINCIPAL INVESTIGATOR: Daniel L. Cox, Ph.D.
Rajiv R.P. Singh

CONTRACTING ORGANIZATION: University of California, Davis
Davis, CA 95616-8671

REPORT DATE: July 2005

TYPE OF REPORT: Annual Revised

PREPARED FOR: U.S. Army Medical Research and Materiel Command
Fort Detrick, Maryland 21702-5012

REPORT DOCUMENTATION PAGE

Form Approved
OMB No. 0704-0188

1. REPORT DATE *(DD-MM-YYYY)*	**2. REPORT TYPE**	**3. DATES COVERED** *(From - To)*
01-07-2005	Annual Revised	15 JUN 2004 - 14 JUN 2005

4. TITLE AND SUBTITLE

Theoretical Modeling of Molecular Mechanisms, Strains, and Time Scales in Prion Diseases

5a. CONTRACT NUMBER

5b. GRANT NUMBER
DAMD17-03-1-0480

5c. PROGRAM ELEMENT NUMBER

6. AUTHOR(S)
Daniel L. Cox, Ph.D., Rajiv R.P. Singh

E-Mail: cox@physics.ucdavis.edu

5d. PROJECT NUMBER

5e. TASK NUMBER

5f. WORK UNIT NUMBER

7. PERFORMING ORGANIZATION NAME(S) AND ADDRESS(ES)

University of California, Davis
Davis, CA 95616-8671

8. PERFORMING ORGANIZATION REPORT NUMBER

9. SPONSORING / MONITORING AGENCY NAME(S) AND ADDRESS(ES)
U.S. Army Medical Research and Materiel Command
Fort Detrick, Maryland 21702-5012

10. SPONSOR/MONITOR'S ACRONYM(S)

11. SPONSOR/MONITOR'S REPORT NUMBER(S)

12. DISTRIBUTION / AVAILABILITY STATEMENT
Approved for Public Release; Distribution Unlimited

13. SUPPLEMENTARY NOTES

14. ABSTRACT

We have obtained significant results modeling: (1) the structure of the minimal infectious prion oligomer as a domain swapped beta helical trimer; (2) metal binding to the prion protein showing results consistent with measured affinities and suggesting a detailed molecular role for the protection of the normal prion form against conversion to the infectious scrapies form when copper is bound to a particular site; (3) kinetics of yeast prion aggregation in vitro illustrating the role of fission; (4) kinetic analysis of transgenic mice time course data for anchorless cellular prions, indicating (a) that the membrane is necessary for exponential growth of infectious aggregate, and (b) that the elongation rate of anchorless prions is likely more rapid than anchored ones. In the coming year we will explore the role of our domain swapped model for 1) understanding strains, 2) understanding a subset of point mutations known to induce disease for those who inherit them,3) possible docking of octarepeats to the beta helical trimers and their role in prion conversion, 4) additional metal binding to the prion protein (iron, sodium, and copper at H111), and (5) the role of the membrane in inducing exponential growth of infectivity.

15. SUBJECT TERMS
Theory/simulations; domain swapping; metal binding and protection, Strain modeling; conversion modeling; kinetics modeling

86

16. SECURITY CLASSIFICATION OF:			**17. LIMITATION OF ABSTRACT**	**18. NUMBER OF PAGES**	**19a. NAME OF RESPONSIBLE PERSON**
a. REPORT	**b. ABSTRACT**	**c. THIS PAGE**			USAMRMC
U	U	U	UU	42	**19b. TELEPHONE NUMBER** *(include area code)*

Standard Form 298 (Rev. 8-98)
Prescribed by ANSI Std. Z39.18

Table of Contents

Revised report for July 2004-June 2005

Introduction

Purpose of Research: To develop theoretical models of prion protein oligomeric aggregation, strains, clearance, and propagation in assistance to the goal of the overall Army prion project of developing early detection schemes. The philosophy is that a theoretical understanding of these different elements of prion science can provide potential strategies for early detection.

Subject of Research (referenced to original approved SOW):

Theoretical modeling of oligomeric aggregation of prion proteins (Task 1 from approved scope of work) – Pertinent accomplishments in Apps. B,C,D,E
Theoretical modeling of Prion Strain Phenomenology (Task II from approved scope of work) – Pertinent accomplishments in App. B
Models for Prion Clearance (Task III of approved SOW) – Pertinent accomplishments in App. E
Models for Prion Propagation (Task IV of approved SOW) – Pertinent accomplishments in Apps. B,D,E

All papers with full citations are contained in the appendix list at the end of this revised report.

Overview

In this second year of our award, we have made significant progress on several areas of theoretical research on the prion problem, particularly on the structure of the minimal prion oligomer and the potential role of domain swapping in that structure, the role of metal binding in potentially protecting against conformational change, and the role of the membrane in determining the kinetics of the disease time course. In terms of our productivity, we have: (i) submitted five papers for publication, one of which have been published, one accepted, and three are under review; (ii) presented seven invited lectures at universities or meetings and three contributed talks at conferences; (iii) co-organized a major international workshop on amyloid diseases (http://i2cam.org/i2camyloid); (iv) received national press coverage for our research on prion diseases (see the attached item in Appendix); (v) a student (Ms. Jianping Pan) has received two different fellowships to

support her research in this area.

In the coming year and final year of the award, building upon the successes emerging from the just completed sabbatical leave of the PI, we plan to explore (i) detailed molecular models for strains in prion disease to be followed by kinetic modeling of strains; (ii) the potential role of the proposed domain swapped prion trimer model in explaining how at least three genetic mutations lead to disease; (iii) binding of other metal ions to the prion protein (notably iron and sodium) and binding of copper to a different site away from the octarepeat regions of the protein; (iv) exploration of a potential role of the octarepeats in converting the cellular prion protein to scrapies form, in formation of non-scrapies based oligomers, and in providing proteinase resistance upon copper binding; (v) modeling the potential role of the neuronal membrane in mediating fission or autocatalysis of the scrapies form of the prion protein.

Key Research Accomplishments

1. ***Proposing a new structure for the minimal infectious unit of prion disease: the Domain Swapped Prion Trimer (DSTP).*** *[General relevance to overall goal of development of an oligomeric aggregation model (Task I of approved SOW); specific relevance to Task 2.d – structural modeling of prion strains.]* This work has been accepted for publication in the Hypothesis section of FASEB Journal and is presented in App. B. One of the more exciting developments in the study of prions in recent years has been the discovery of areal aggregates of infectious oligomers in electron microscopy work by the UCSF group (see refs. 3, 4 of App. B). In Ref. 4 of App. B, the UCSF group boldly proposes that the infectious oligomers are trimers of left handed β–helices with a similar shape and size to the bacterial carbonic anhydrase trimer (ref. 5 of App. B), and that these oligomers can readily stack into fibrils. The difficulty with this proposal lies in understanding what stabilizes the proposed β–helical Prion Trimer (BPT): while the carbonic anhydrase possesses three zinc ions which covalently bond to histidines on different monomers, there is nothing analogous for the BPT. We note in this paper that domain swapping, implicated elsewhere in amyloid formation (see Refs. 11-13 of App. B) can stabilize the trimer by affording hydrogen bonding in the central region (Fig. 1 of App. B). Using all atom MD simulations, we showed that this structure is held together by a significant hydrogen bonding network (Fig. 2 of App. B) similar to the serine acyltransferase

trimer (ref. 9 of App. B, also studied as a control in our paper), compatible with the external α-helices of the BPT model (Fig. 3 of App. B), is remarkably stable to temperature (which blows the BPT structure apart—see Fig. 4 of App. B), and may provide insights into the conformational details of prion strains (p. 19 and Fig. 5 of App. B) and three mutations implicated in heritable prion disease (discussion on p. 19 of App. B). We discuss these latter points further in our discussion of research plans for the coming year. We regard the DSTP model as an important modification to the proposed BPT structure for the infectious prion protein. This work was carried out in collaboration with S. Yang, H. Levine, and J. Onuchic from the Center for Theoretical Biological Physics at UC San Diego, a fruitful collaboration for the PI which will be carried forward in the coming year.

2. ***Comprehensive computational study of metal binding to the prion protein and demonstration of a potential role of copper binding in inhibiting conversion of the prion protein.*** *[General relevance to Task I of approved scope of work – metal binding can provide potential detection mechanisms via ESR and SPECT, and can disrupt aggregation as per the arguments in the paper.] [Note: a shortened version of this work discussing only the influence of copper on inhibiting aggregation appeared in Biophys. J.]* In this work, with manuscript submitted to Journal of Molecular Biology and presented in App. C, we have performed a fully Quantum Mechanical electronic structure study of the binding of several divalent transition metal ions to the prion protein and explored the potential implications of such metal-binding to the normal function of the prion-protein and to their role in prion-diseases. We find that metal ions bind to at least two different regions of the prion protein: (i) the highly conserved HGGGW sequence in the octarepeat region near the N-terminal and (ii) the GGGTH sequence in the region of the protein that is believed to convert to the beta-sheet form in course of the prion diseases (For location of the sequences in the human prion protein See Fig. 1 of the manuscript in App. C). For the HGGGW sequence, the binding energy trend found in our studies for different transition metal ions, reported in Table 2 of the manuscript in App. C, is consistent with in vitro measurements, and can be plausibly explained by Jahn-Teller and electrostatic mechanisms compatible with the well known Irving-Williams series for binding affinities of transition metal ions with polydentate ligands. The coordination geometry of copper ion in the octapeptide region (See Table 1 and Figs. 2 and 3 of manuscript in App. C), agrees well with Electron Paramagnetic Resonance (EPR) and X-ray crystallography measurements. We also find that GGGTH sequence binds

much more strongly, consistent with separate experiments. Two of our findings may have particularly important implications for the (normal) cellular function and disease-causing role of the prion protein: (i) We find that metal-binding affinity and associated peptide conformations are strongly dependent on protonation states of the peptides, implying that pH changes can modulate metal-binding and protein conformation (See Figs. 2 and 3 of the manuscript in App. C). (ii) We find that the metal-bound conformation is incompatible with the misfolded disease causing (infectious) structure proposed by Govaerts et al (See Ref. 16 and Fig. 5 of the manuscript in App. C for comparison details). These findings suggest that copper needs to be expelled from the protein before the beta-sheet rich misfolding can occur. This is, indeed, consistent with experimental findings of copper depletion in infected and diseased tissues (ref. 20 of App. C) and that copper suppresses *in vitro* amyloid formation. Overall, our studies are consistent with the idea that metal ions, such as copper, play a complex role in prion diseases. They may play a protective role in the disease by creating a disease-incompatible structure and thus enhancing the barrier to misfolding. However, the structure may be protease resistant, and this may enhance disease propagation. This work has been submitted to the Journal of Molecular Biology.

3. ***Detailed modeling of* in vitro *yeast prion aggregation*** *[Of general relevance to Task I of original SOW, of specific relevance to Task 3.b (developing spatially explicit kinetic models), Task 4.b (development of kinetic models for propagation), and as a warmup to task 2.b, developing kinetic models of prion strains.]* The importance of yeast prions, in the field of prion diseases, arises from the fact that several key concepts of mammalian prion propagation have been validated, by studying relatively harmless yeast proteins in the laboratory. These include fission and exponential growth, in vitro generation of infectious agent, and existence and propagation of strains. Detailed modeling of yeast-prion kinetics allows one to highlight the similarities and differences between yeast and mammalian prions, which may be important for controlling the disease. In this work, with manuscript submitted to Physical Review E and presented in App. D, we present a model of yeast prion aggregation that can account for almost all aspects of in vitro kinetic data that show (i) Linear aggregates which grow by monomer addition, (ii) A modest dependence of the lag-time on monomer concentration varying nearly as an inverse square-root function (See Fig. 2 in the manuscript presented in App. D), (iii) Sigmoidal growth of aggregates that is nearly exponential, and (iv) A distribution of aggregate sizes with a

mode that is large (10s-100s of monomers). We have contrasted our simulation work done via kinetic equations (Figs. 3,4,5,6 in the manuscript presented in App. D) and by stochastic algorithms (Figs. 7,8,9 in the manuscript in App. D) with alternative models of aggregation that do not include fission and hence fail to obtain the exponential growth. We have also shown that fission leads to a distribution of aggregate sizes that is Weibullian (See Fig. 4 and Fig. 9 in the manuscript presented in App. D), which may be tested in future experiments. In comparing the yeast-prion kinetics to the mammalian case, we find two important differences. The first is that mammalian prions may form two-dimensional *areal* aggregates rather than one-dimensional ones. A more significant difference seems to be the role of membranes in fissioning and exponential growth, which is not necessary in the yeast case, allowing spontaneous fission to take place in vitro. It is clearly important to further investigate the role of membrane in fissioning of mammalian prions.

4. ***Demonstration of the necessity of the membrane in exponential* in vivo *growth of prion infectivity.*** *[General relevance to Task I of SOW (infectious oligomer aggregation requires membrane binding to spread disease), general relevance to Task III (clearance requires membrane binding), general relevance to Task IV (disease propagation with attendant exponential growth requires membrane binding)] [Note: this work was published in Biophys. J.]* This work has been submitted as a technical comment to Science and is contained in App. E. We respond here to a beautiful paper by Chesebro *et al.* (ref. 1 of App. E) showing that membrane anchoring is necessary for cell toxicity/clinical symptoms in mammalian prion disease by working with transgenic mice lacking the sequence necessary for attaching the GPI anchor of the prion protein. At the same time, the animals remain infectious! We point out several issues in our comment: (i) Data from Chesebro *et al.* showing the time course of prion infectivity in the transgenic mice is very well fit by a quadratic-in-time dependence *over the full 600 days of observation (!)* (Fig. 1 and Eq. 1 of App. E), consistent with simple elongation kinetics described by Ferrone (refs. 3, 4 of App. E) without (a) monomer depletion or (b) fission/exponential growth. The significance of this result is that the membrane anchoring must play a crucial role in generating the exponential growth characteristic of prion disease. (ii) We extend the argument to infer that the fundamental elongation rate for wild type aggregates (with membrane anchors) is likely to be significantly slower than in the anchorless case and attribute this to what is most probably a slower clearance rate for the anchorless PrP^C proteins (Eq. 2 and discussion on p. 76 of App. E). This result helps to explain why

mice heterozygous for anchor-full and anchorless PrP^C display faster incubation times at a given dose than wild type mice.

5. ***Review of amyloidogenic proteins from a materials perspective.*** In this paper, presented in App. F and published in the June 2005 issue of the Materials Research Bulletin, we have put forward a review of the proteins implicated in amyloid diseases from a materials science perspective. While this does not represent new research, it does represent a significant intellectual effort aimed at communicating our research interests to a much broader scientific audience.

Research Directions for Coming Year

1. ***Correlation of relative mutant hydrophobicity with incubation time and DSTP stability.*** We have initiated discussions with Glenn Telling and Karah Nazor of the University of Kentucky about understanding their Tg mice data for mutations at P101 using our DSTP model. They find in mice overexpressing the PrP protein that mutation at P101 (implicated, e.g., in the P102L mutation leading to GSS in humans) to residues more hydrophobic than P (notably L and I) induces spontaneous prion disease with incubation times roughly correlating with hydrophobicity. Within our DSTP model, this may be potentially be rationalized by the following observations: (i) for PrP^C, substituting a relatively more hydrophobic residue for P102 will partially destabilize the structure since this is in a solvent exposed region; (ii) for our DSTP PrP^{Sc} model, the substitution can have two effects, (a) generically rendering the proline containing hinge region of our DSTP more flexible and thus potentially lowering the barrier to conversion by increasing the search rate of the protein, (b) affording solvent exclusion in the core region and thus stabilizing the DSTP relative to the WT form. In the latter case, a simple two state model (which is admittedly an oversimplification) displays a linear relationship between the change in the free energy difference between cellular and scrapies form of the protein and the lowering of the barrier. Our goal here is to carry out all atom MD simulations on both cellular and DSTP forms of the prion protein and compare to the incubation time data of Telling and Nazor to assess the molecular basis for the correlation with relative hydrophobicity. This will be carried out in collaboration with S. Yang, H. Levine, and J. Onuchic at UCSD.

2. ***Modeling of strain conformations and kinetics within the domain swapping picture.*** As noted in App. B, the introduction of domain swapping opens up intriguing conformational possibilities for the explanation of strains in prion disease, the simplest of which is that the number of monomers in a domain swapped oligomer encodes strain. If this is so, strains will be able to breed true by either (i) oriented areal aggregation on a membrane surface or (ii) by interneuronal templating across (most likely) the synaptic cleft. In addition to this simple idea, there are three other ideas worth exploring within this general picture: (a) Strain conformation is encoded within the `splay' of the left handed β-helices—the helices of carbonic anhydrase are for example rather straight, while those for serine acyltransferase are splayed inward from C-terminus to N-terminus. This idea could account for why some strains have associated amyloid plaques and others don't, since splay will mitigate against stacking due to the epitaxial mismatching between the helical ends. (b) Strain conformation is encoded in the cross sectional shape of the left handed β-helix. While most of the 20 non-redundant left handed β-helices found on the pdb possess triangular cross section, one has two sides (the collagen binding domain of yersinia adhesion YadA, pdb code 1P9H). It is worth exploring whether such a two sided helix might be possible for the prion protein. (c) Domain swapping occurs with the major loop of the prion. Cohen and Prusiner (Ref. 19 of App. B) have earlier suggested that different domain swaps might correspond to different strains. In this light it is interesting to consider the possibility of domain swapping via the major loop of the BPT structure. This would be ineffective for strains which can take the `miniprion' PrP^{Sc} 106 form, but is worth exploring. We will first explore possibility (a) and examine in particular the stability of different dimers and tetramers. Assuming we find stability for the different possible strain conformations, we will develop stochastic kinetic models for both areal aggregation and interneuronal templating to assess the feasibility of this simple picture describing time course kinetics.

3. ***Possible docking of octarepeats with left handed β-helices and implications for cellular-to-scrapies conversion.*** Zahn has shown that the octarepeat region of the prion protein with copper bound may represent a new structural motif (Ref. 21 of App. C). Intriguingly, three octarepeats yield a structure resembling two sides of an equilateral triangle with cross sectional area approximately that of the

standard left handed β-helix. This suggests a potential role for docking of the octarepeat on the left handed β-helix of a scrapies form prion which could be important in templating the cellular form of the prion for conversion. We intend to study this docking possibility with all atom molecular dynamics and subsequently explore the implications for the conversion process. We note that while octarepeats are not *necessary* for infection, they do enhance incubation time relative to transgenic animals lacking them, and additional (>4) octarepeats induce heritable disease. Hence, the presence of octarepeats clearly enhances the tendency towards conversion to scrapies form.

4. ***Metal ion binding and structural modulation of the prion protein.*** Besides the Cu, Ni, Mn, Zn ions already studied, we will look at binding of: (i) *Fe to the prion protein.* This is motivated by work by Singh and collaborators[1] who have shown that the prion protein co-transports across epithelial cells with ferritin. (ii) *Na to the prion protein.* This is motivated by the work of Nishina *et al.* (Ref. 48 of App. C) who have shown that in solution both Na and Cu can confer enhanced proteinase K resistance to the truncated PrP 27-30 scrapies form. Since nominally Na is monovalent and larger than Cu, the binding mechanism if any is mysterious and we will examine potential binding sites and their implication for PK resistance. In addition, we will explore how Cu binds to the H111 residue as claimed in Ref. 12 of App. C.

5. ***Modeling of membrane mediated fission and oligomeric autocatalysis.*** Our work in App. E strongly suggests that the membrane plays a role in engendering exponential growth of prion infectivity. This can either arise from fission of aggregates, or from autocatalysis. The former case clearly applies for *in vitro* yeast prion. We propose to explore two potential mechanisms for membrane mediated fission, both deriving from Ginsburg-Landau modeling of the membrane bound prion aggregates. In the first, we will examine whether curvature near the edges of the synaptic cleft can break aggregates. These areal aggregates are presumably less strongly bound than individual oligomers. A separate possibility is that membrane undulations can break up rafts. Our colleague Prof. Atul Parikh at UC Davis, studying the raft like structures which can bind other GPI proteins has come to this conclusion. We can initiate some combined theory/experiment studies with Prof. Parikh on this matter. In addition, assuming there is some population of ``soft oligomers'' from the cellular form of the prion protein, there

can be autocatalytic interneuronal templating of scrapies form, and we will attempt to simulate this.

Additional Research Results

Last year we discussed a study of the membrane insertion properties of the prion protein, particularly because the known transmembrane segments of the prion proteins contain a mutation (A117V) implicated in GSS. We carried this out with the segment of prion protein from residue 90-153, which contains both known transmembrane domain (residues 111-134), the primary β-helical region of the BPT and DSTP models discussed above, and of course, residue 117. We did study this using the membrane insertion program used earlier by our group for a study of the insertion of Aβ peptides. However, we found nothing using the program which was surprising, unlike the Aβ. In particular, (i) whether initiated in the membrane or outside the membrane, the transmembrane sequence reached the same α-helical structure, which this particular code is biased towards producing; (ii) the A117V mutation has no significant effect within the simulation.

We initiated a study of the possibility of using Cu or Mn isotopes for either PET or SPECT studies for early prion detection, but put that aside when the DSTP study opened up multiple research directions.

Reportable Outcomes: Awards, Activities, Presentations and Publications

1. **Awards, Activities, and Presentations** ***(Appendix A)***
2. **Structure of Infectious Prions: Stabilization by Domain Swapping** ***(Appendix B) Published as S. Yang, H. Levine, J. Onuchic, D.l. Cox, FASEB J 19, 1778-1782 (2005)***
3. **An *ab initio* Electronic Structure Study of Transition Metal Binding to the Cellular Prion Protein** ***(Appendix C) Shorter version published as D.L. Cox, J. Pan, R.R.P. Singh, ``A mechanism for copper inhibition of infectious prion conversion,'' Biophys. J. 91, L11-L13 (2006)***
4. **One Dimensional Model of Yeast Prion Aggregation** ***(Appendix D) Published as K.C. Kunes, D.L. Cox, R.R.P. Singh, Phys. Rev. E72, 051915 (2005)***
5. **Comment on "Anchorless Prion Protein Results in Infectious Amyloid**

Disease Without Clinical Scrapie" ***(Appendix E) Published as D.L. Cox, R.R.P. Singh, S. Yang, ``Prion Disease: Exponential Growth requires Membrane Binding'', Biophys. J. 90, L77-79 (2006)***

6. **The Materials Science of Protein Aggregation** ***(Appendix F) Published as D.L. Cox, H. Lashuel, K.Y. Lee, and R.R.P. Singh, Materials Res. Bull. 30, 79-84 (2005)***
7. **Yahoo! News Search Results for Cox Singh "mad cow"** ***(Appendix G)***

Conclusions

In summary, this year we have (i) produced a new model for the minimal prion oligomer; (ii) modeled the affinity trend and structure of copper binding to the prion protein and shown that the conversion to left handed β-helical structure of the scrapies form requires expulsion of the nonoctarepeat copper consistent with post mortem studies, cultured neuron studies, and in vitro amyloid growth studies; (iii) in vitro yeast prion kinetics can be well described by a simple stochastic growth model with fission; (iv) the membrane is critical for exponential growth of prion infectivity and without membrane anchoring prion aggregate elongation is more rapid. We propose a number of studies following from this work towards (i) understanding the conformational nature and kinetics of strains; (ii) understanding how mutations to P102,105 can induce heritable disease; (iii) how unusual structure of the octarepeat region can play a role in templating conversion of cellular to scrapies form of the prion disease; (iv) how Fe and Na ions might bind to the prion protein, and how copper may bind to H111; (v) how the membrane can play a role in engendering exponential growth of infectivity.

References

[1] Mishra, R.S., Basu, S., Gu, Y., Luo, X., Zou, W., Mishra, R., Li, R., Chen, S.G., Gambetti, P., Fujioka, H., and Singh, N. (2004) Protease resistant human prion protein and ferritin are co-transported across Caco-2 epithelial cells: Implications for species barrier in prion uptake from the intestine. *J. Neurosci.* **24**, 11280-11290.

APPENDIX A: ACTIVITIES, HONORS, AND PRESENTATIONS ASSOCIATED WITH THIS RESEARCH AWARD

Honors

J. Pan I^2CAM Junior Fellow (supported collaborative visit with Prof. E. Artacho, Cambridge University, Jan-Feb. 2005)

J. Pan UC Davis Summer Graduate Research Fellow (supports one month of summer research, Summer 2005)

Activities

D.L. Cox, R.R.P. Singh, co-organizers of First International ICAM Workshop on ``**PROTEIN AGGREGATION AND AMYLOID FORMATION IN SYSTEMIC AND NEURODEGENERATIVE DISEASE: PHYSICAL, MOLECULAR AND BIOLOGICAL APPROACHES**,'' Lausanne, Switzerland, July 16-19 2005. (http://i2cam.org/i2camyloid)

Invited Presentations

D.L. Cox:

- ``*Molecular level modeling of the prion protein,''* Brooks group seminar, Scripps Research Institute, June 2005.
- ``*Consider a spherical mad cow: a physical look at prions,*" Condensed matter theory seminar, Department of Physics, The Ohio State University, April 2005.
- ``*Consider a spherical mad cow: a physical look at prions,*" Condensed Matter Journal Club, Department of Physics, UC San Diego, March 2005.
- ``*Physical Modeling of Amyloid Diseases*," invited lecture, Symposium on Frontiers in Computational Biology, Rice University, December 2004.
- ``*Physical Modeling of Amyloid Diseases,*" seminar, Center for Theoretical Biological Physics, UC San Diego, November 2004.

R.R.P. Singh:

- "*Prion Diseases*", Seminar at Jawaharlal Nehru University, Delhi, India, July 2004.
- "*The mysterious prion protein*", Mathematics Department Seminar, University of California at Davis, November 2004.

J. Pan:

- ``*Theoretical study of metal binding to the cellular prion protein,''* Seminar, Biophysics Graduate Group, UC Davis, November 2004.

Contributed Presentations:

D.L. Cox, ``*Theoretical investigation of metal binding affinities in the prion protein*,'' Keystone Symposium on Transmissible Spongiform Encephalopathies, Snowbird, Utah, January 2005.

K. Kunes, *Kinetic and Stochastic Models of 1D yeast ``prions"*, American Physical Society March Meeting, Los Angeles, March 2005. (http://meetings.aps.org/Meeting/MAR05/Event/21907)

J. Pan, *Theoretical study of metal binding in the Prion protein*, American Physical Society March Meeting, Los Angeles, March 2005. (http://meetings.aps.org/Meeting/MAR05/Event/21906)

The FASEB Journal • Hypothesis

Structure of infectious prions: stabilization by domain swapping

Sichun Yang,* Herbert Levine,* José N. Onuchic,* and Daniel L. Cox*,†,[1]

*Center for Theoretical Biological Physics, University of California San Diego, La Jolla, California, USA; and †Department of Physics, University of California, Davis, California, USA

ABSTRACT **A candidate structure for the minimal prion infectious unit is a recently discovered protein oligomer modeled as a β-helical prion trimer (BPT); BPTs can stack to form cross-β fibrils and may provide insight into protein aggregates of other amyloid diseases. However, the BPT lacks a clear intermonomer binding mechanism. Here we propose an alternative domain-swapped trimeric prion (DSTP) model and show with molecular dynamics (MD) that the DSTP has more favorable intermonomer hydrogen bonding and proline dihedral strain energy than the BPT. This new structural proposal may be tested by lysine and N terminus fluorescent resonance energy transfer (FRET) either directly on recombinant prion protein amyloid aggregates or on synthetic constructs that contain the proline/lysine-rich hinge region critical for domains to swap. In addition, the domain swapping may provide *1)* intrinsic entanglement, which can contribute to the remarkable temperature stability of the infectious prion structure and help explain the absence of PrP^{Sc} monomers, *2)* insight into why specific prolines are potentially relevant to three inherited forms of prion disease, and *3)* a simple explanation of prion strains assuming the strain is encoded in the monomer number of the oligomers.—Yang, S., Levine, H., Onuchic, J. N., Cox, D. L. Structure of infectious prions: stabilization by domain swapping. *FASEB J.* 19, 1778–1782 (2005)**

Key Words: prion · domain swapping · β-helix · amyloid

MODEL β-HELICAL PRION TRIMER

THE PROTEIN-ONLY MODEL for prion diseases remains the leading candidate to explain the infectious form of the disease (1), and this has been significantly strengthened by the successful production of disease from synthetic prion protein aggregates (2). Clearly, the understanding of prion disease pathology, propagation within the body, and therapeutic approaches will be greatly enhanced by a detailed knowledge of the structure of the minimal infectious protein unit.

The discovery of areal aggregates of infectious prion protein oligomers in purified brain extracts from mice has inspired a leading candidate model for the minimal infectious unit, a trimer in which large portions of the N terminus are converted to left-handed β-helices (3, 4). We call this the β-helical prion trimer (BPT) model. **Figure 1*A*** shows a top view of the BPT in the β-helical region. This BPT displays a 3-fold symmetry consistent with maps of the electron density difference between the PrP 27-30 oligomers and the "miniprion" $PrP^{Sc}106$ oligomers. The BPT can easily be stacked to form filaments, which can then be wound into amyloid fibrils. The model trimer also shares detailed structural features with the bacterial protein carbonic anhydrase trimer (5). Inspired in part by this model, others have explored the possibility that the β-helix plays a role in other amyloid structures such as aggregates of polyglutamine peptides (6), β-amyloid peptides (7), and yeast prion-like proteins (8).

However, it is not clear in the BPT model what holds the trimer together. The carbonic anhydrase trimer, which was the template for the BPT model is in fact held together by intermonomeric covalent bonding of zinc ions (5), which are not present in PrP^{Sc}. It was suggested that a hydrogen bonding network is responsible for this binding (4), as in the case of the bacterial β-helical trimer serine acyltransferase (SAT) (9), but no effort was made to test this idea quantitatively. Moreover, the yellow loops of the BPT model (which are highly conserved (10)) shown in Fig. 1*A*, *B* and expanded in Fig. 1*C* contain two prolines, and prolines tend to disfavor this type of bending.

HYPOTHESIS: A DOMAIN-SWAPPED PRION TRIMER IS THE MINIMAL INFECTIOUS UNIT

We hypothesize that a stable oligomeric structure for the infectious prion is the domain-swapped trimeric prion (DSTP) of Fig. 1*B*, which can increase hydrogen bonding and reduce elastic energy relative to the BPT structure proposed earlier. Further, we conjecture that the DSTP structure may be relevant to *1)* the unusual temperature stability of the prion protein and the lack of observation of PrP^{Sc} monomers (both due to the entanglement of the DSTP structure), *2)* the kinetics of at least three inherited forms of human prion disease, and *3)* the encoding of prion strains in conformation.

[1] Correspondence: CTBP, UC San Diego, MC 0374, 9500 Gilman Dr., La Jolla, CA 92093-0374, USA. E-mail: cox@physics.ucdavis.edu

doi: 10.1096/fj.05-4067hyp

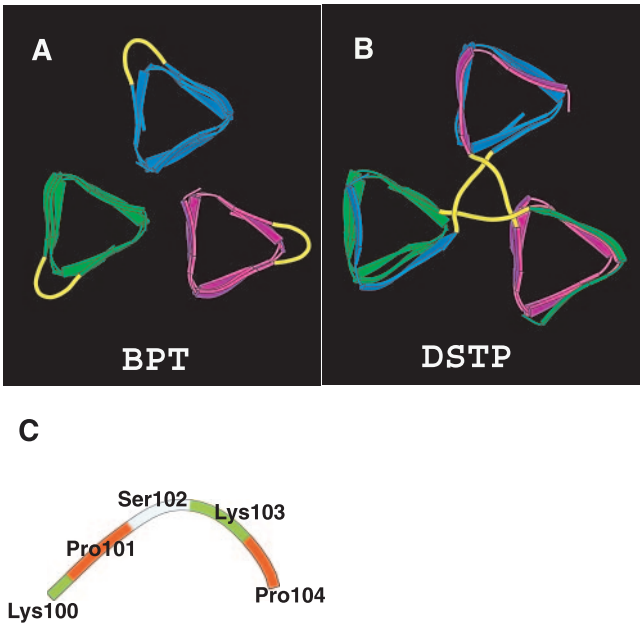

Figure 1. *A)* Proposed β-helical structure of the truncated $PrP^{Sc}106$ prion trimer (BPT) taken from ref 4 (residues G89-F140). *B)* Structural model of domain-swapped trimeric prion (DSTP) of the present paper. *C)* The proposed hinge region expanded from the yellow loops in panels *A*. *B*.

DOMAIN SWAPPING: MOTIVATION AND RESULTS

Concern with stability of the BPT model led us to modify it by domain swapping (11–13), especially since prolines are present in the hinge or bridging regions of several proteins that domain swap (14). For example, in p13suc1, the strain on two prolines in the hinge modulates the equilibrium between monomers and domain-swapped dimers (15, 16).

We constructed our DSTP model of Fig. 1*B* from the proposed BPT structure (we thank C. Govaerts for providing his coordinate file) by reorienting the monomers to place the loop regions near the trimer center and swapping residues 89-99 to a neighboring β-helix in a cyclical fashion, with the BPT loops serving as hinges. This DSTP model straightens these loops, adds more possible hydrogen bonds in the loop region, and preserves the putative monomer-monomer spacing and 3-fold symmetry of the electron density maps (3). We ran all-atom, explicit solvent MD (see Appendix for details) on energy minimized DSTP and BPT structures using AMBER8 (http://amber.scripps.edu). As a control, we applied the same protocol to the serine acyltransferase (SAT) β-helical trimer, which has no strained prolines and for which there is direct crystallographic evidence for intermonomer hydrogen bond-mediated cohesion (9). Wee also carried out two other simulation tests: *1)* we examined the stability of the DSTP model with the inclusion of the C terminus α-helices proposed in ref 4, and *2)* we carried out three distinct 1-ns runs for both the BPT and DSTP structures to make sure there is no special circumstance with regard to individual simulations.

We have concluded that the DSTP is significantly more stable than the BPT and therefore a more promising candidate structure. First, we have enumerated direct and water-bridged hydrogen bonds between monomers in the BPT model, our DSTP model, and the SAT structure (see Appendix), and carried this out for three separate MD runs on each structure. We show the direct hydrogen bond counts for three different 1-ns runs of the BPT and DSTP structures in **Fig. 2**. For the BPT, we find 2 ± 1, 5 ± 1, and 2 ± 1 direct hydrogen bonds for the three runs (averages over the last 100-ps of simulation time), and at the last simulation time 0, 0, and 1 water-mediated hydrogen bonds. For the DSTP, we find for all three runs 9 ± 1 direct hydrogen bonds for the last 100-ps of simulation time and 2, 1, and 1 water-mediated hydrogen bonds in the last simulation snapshot. In the one BPT case with a relatively high number of direct hydrogen bonds, the N terminus from one monomer has contacted with the N terminus region of another. In general, the BPT hydrogen bonds form around Q89 only, while the DSTP hydrogen bonds form in the hinge region. Note that Fig. 2 shows direct hydrogen bonds formed in the monomer-monomer interface for the DSTP to generically increase with time while those from the BPT generically decrease with MD time. In contrast to the BPT, the simulated β-helical portion (F140-A237) of the SAT trimer has 11 direct and 3 water-bridged hydrogen bonds (after two stage equilibration with no restraints).

Second, we remark that the domain swapping also relaxes the P101 and P104 dihedral energy by ~1.0 kcal/mol after 1-ns of MD. Hence, the domain swapping helps relieve elastic strain as anticipated.

Third, we have verified that the DSTP structure for the $PrP^{Sc}106$ can accommodate the C terminus α-helices without affecting stability. This is a nontrivial point, since a rigid rotation of the monomers within the BPT is not possible due to steric constraints. As shown in **Fig. 3**, we find that by "peeling off" one triangular edge (residues 133-140) of the lower (C terminus) end of each β-helix to form a random coil segment that we can link to the α-helices that begin at residue 177, with no resultant change in direct hydrogen bonding structure.

Finally, high temperature MD provides direct evidence for BPT instability; at 500K, the DSTP remains

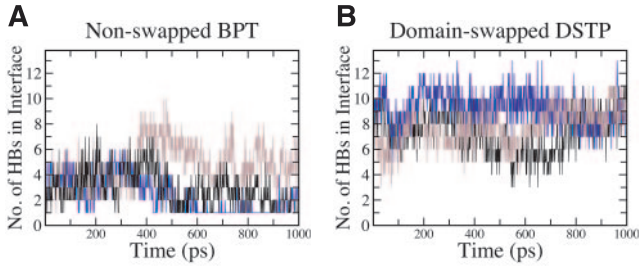

Figure 2. MD simulations show that the nonswapped BPT (*A*) has less direct hydrogen bonds in the interface region than the domain-swapped DSTP (*B*). In both cases we have simulated residues G89-F140. Different colors correspond to three different 1 ns MD runs in each case initialized at different initial temperatures (see Appendix).

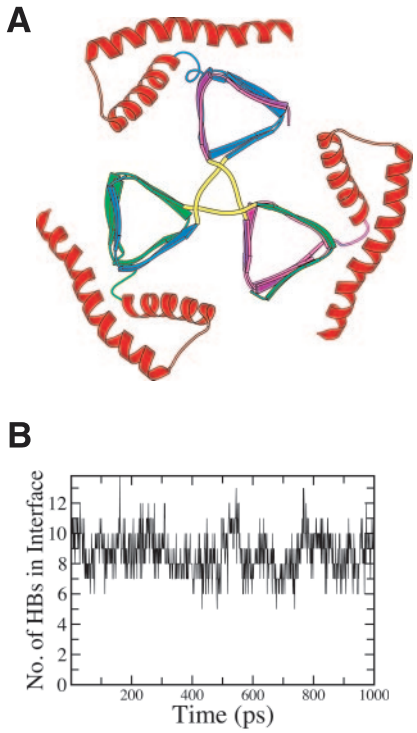

Figure 3. *A)* Model for DSTP $PrP^{Sc}106$ (with residues G141-H176 deleted) and α-helices included. Residues 133-140 have been removed from the lower rung of the β-helices for each monomer, converted to random coil, and attached to residue 177 of the α-helices. *B)* Number of direct hydrogen bonds for the DSTP structure with intact α-helices. The α-helices have no effect on the stabilization induced by the domain swapping.

compact and entangled, while the BPT monomer-monomer separation nearly doubles. Principal component analysis, which identifies the amplitude and character of the dominant fluctuations, shows similar BPT unbinding tendencies at 300K as in the 500K simulation, but no unbinding tendencies for the DSTP. **Figure 4** shows the radius of gyration in the 500K runs as a function of simulation time. Within the 1-ns window of simulation, the BPT radius appears to keep growing, reaching about twice that of the apparently more stable DSTP structure. This stabilization through entanglement may be relevant to the unusual temperature stability of infectious prion proteins, although we cannot rule out that such stabilization is related to larger scale aggregates of prion oligomers. The entanglement may also be relevant to the inability to isolate monomeric forms of PrP^{Sc}, since the scrapies form is stabilized in this picture only in aggregate.

POSSIBLE RELEVANCE TO INHERITED DISEASES AND PRION STRAINS

Finally, we discuss the possible relevance of the DSTP model to inherited diseases and strains. First, proline point mutations yield heritable Creutzfeldt-Jakob disease (P105T for humans, P104T for mice) or Gerstmann-Sträussler-Scheinker disease (P102L, P105L for humans, P101L, P104L for mice; see chapter 14, ref 1). Transgenic mice with P101I have even greater disease susceptibility whereas those with P101Y have somewhat less susceptibility than P101L (K. Nazor and G. Telling, private communication). We note that the centrality of these sites in the DSTP hinges affords possible burial of the relatively hydrophobic I, L, T, and Y side chains and a potential speed up of trimer formation through increased hinge flexibility. Moreover, the insertion of relatively hydrophobic residues into the unstructured region of the normal PrP^{C} protein will raise the energy of this structure. Indeed, it is already known that the P102L mutation is marginally less stable than the wild-type protein (see p. 694, ref 1). A decrease in the stability of the cellular protein form relative to wild-type monomers coupled to an increase in stability of the scrapies form (associated with more effective hydrophobic burial of the mutant residue) should lead to more rapid conversion kinetics via ramping of the overall free energy surface slope in favor of the scrapies form.

In **Fig. 5** we illustrate two ways in which strains might breed true if the monomer content within an oligomer encodes the strain information. With this assumption, strains can breed true either by *1)* oligomer conversion and crystallization on membranes (Fig. 5*A*), with local shape matching favoring homogeneous growth in a manner analogous to the oriented aggregation of nanoparticles (17), or *2)* via interneuronal, epitaxially templated conversion across the synaptic cleft or interneuronal gaps (Fig. 5*B*). The plausibility of the latter conjecture rests on the length of unstructured N terminus PrP^{C}, which is ~100 residues, or ~30 nm stretched out, easily sufficient to span the interneuronal gaps of 10–20 nm. Both of these models would enjoy enhanced conversion kinetics in the presence of unconverted or "soft" oligomers of PrP^{C} (18); the interneuronal mechanism in this case would allow for exponential growth via oligomeric autocatalytic conversion. We note that a different domain swapping model

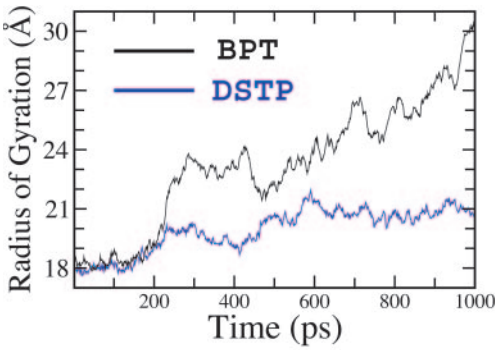

Figure 4. The entanglement due to domain swapping introduces additional stability for the DSTP relative to the BPT as revealed by high temperature (T=500K) simulations, where the radius of gyration of the BPT increases more rapidly than that of the DSTP, which reflects unbinding of the BPT. Principal component analysis at 300K reveals a similar unbinding tendency.

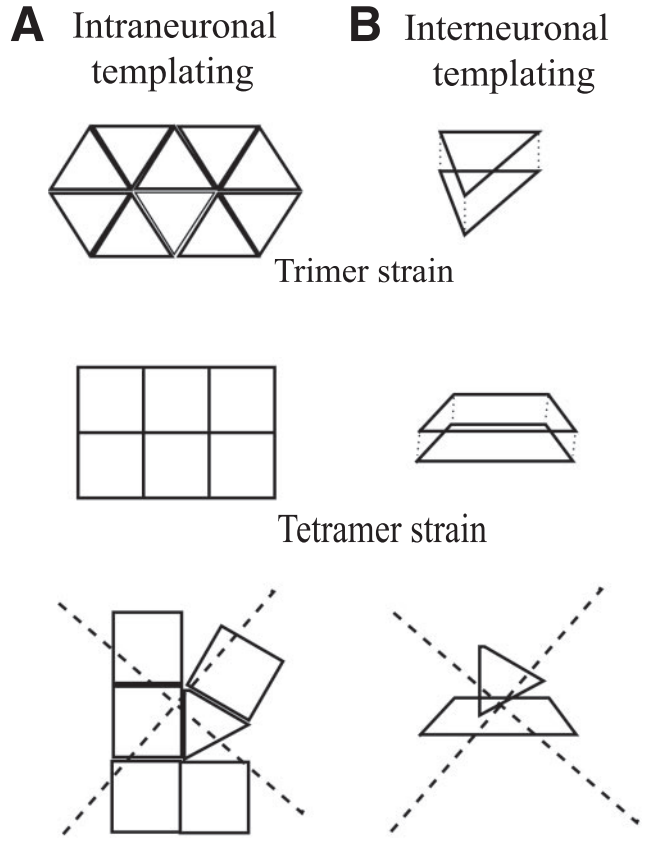

Figure 5. Schematic models for strains breeding true under the assumption that strain is encoded in monomer number. For simplicity, we assume one strain is encoded as trimers, one as tetramers. *A)* Areal aggregation. Given local size or orientation mismatches between trimers (upper image) and tetramers (lower image), energetics will, for example, disfavor growth of trimers off of tetramer seeds (lower image). *B)* Interneuronal templating. Assuming that seeds template conversion across interneuronal gaps or the synaptic cleft, trimers will seed trimer growth (upper image), tetramers will seed tetramer growth (middle image), and there will be no cross-seeding between trimers and tetramers.

for strains has been conjectured previously (19); separately, domain-swapped prion dimers have been crystallized (20). The latter result is consistent with prion oligomerization via intermolecular disulfide bonding as has been shown by redox induced prion fibrillization in vitro (21), although only intramolecular disulfide bonding has so far been observed in vivo (22). Other specific domain swapping mechanisms than those we have discussed here may play a critical role in amyloid fibril formation for prions as has been observed for other proteins (24–26). For the PrP 27-30 scrapies form, the large loop (residues E145-R163) of ref 4) made from some of the deleted residues of the $PrP^{Sc}106$ structure could serve as a hinge region for alternative domain-swapped structures.

PROPOSED EXPERIMENTAL TESTS

While the DSTP structure may ultimately be testable directly on recombinant infectious prion oligomers, as have been synthesized by Prusiner and collaborators recently (2), we first propose testing an analog system by FRET labeling. Poly-Q peptides are of considerable interest because of the polyglutamine diseases (especially Huntington's). The "critical" length near 36 glutamine repeats for disease is suggestive of a left-handed β-helix structure, as discussed elsewhere (4, 6, 27). The key experiment we propose is to construct synthetic peptides of the form Q12(KPSKPK)Qm, where m = 24–36. The goal is to label the N terminus Q's in half the peptides with a donor, the K's with a different donor, and in the other half put in N terminus Q acceptors and K acceptors. If the argument about stress relaxation and hydrogen bond stabilization works for the prion, it should also work here. There should be intense K-K FRET given intermonomer separations of the side chains by ~4 Å if the domain swapping arises. There will also be weak N terminus-Q- N terminus-Q FRET. Presumably there could be an N terminus-Q-to-N terminus-Q FRET signal arising with time if the trimers are first formed and then they fibrillize, since the corresponding distances would get reduced by ~60% case assuming stacking of the β-helices. If this works on the synthetic peptide it should be attempted on recombinant prion protein prior to in vitro aggregation as per ref 2. We would anticipate little interfering contributions from other lysines in the prion protein sequence that are far from the hinge region.

SUMMARY

We propose a domain-swapped trimer model for the minimal infectious prion oligomer, and note that the domain swapping stabilizes the oligomer relative to the earlier proposed model by reducing stress in proline containing loops, increasing intermonomer hydrogen bonding, and promoting entanglement. We conjecture that domain swapping may play a role in explaining the temperature stability of the scrapies form of the prion protein, the absence of PrP^{Sc} monomers, inherited prion disease phenotypes associated with mutating prolines in hinges of the DSTP, and that conformation may be encoded in the monomer number in a given oligomer. Finally, we propose experimental tests based on FRET labeling of principally lysine residues near the crucial pralines, which should produce intense FRET response if the domain swapping is present. FJ

Appendix

The simulations were carried out with the AMBER8 molecular dynamics package (28) with the AMBER parm99 force field and explicit TIP3P waters, following these procedures. *1)* Before we start a molecular dynamics simulation, we perform an energy minimization of 2000 steps to partially relax the entire molecular system. *2)* We perform a two-stage equilibration to further relax the protein and the surrounding solvent. In the first stage, we start the system from a low temperature

of approximately 100K and gradually heat up to 300K over 20-ps of simulation time. We perform this stage of equilibration with the volume held constant. In the second stage, we equilibrate the system using pressure and temperature control to adjust the density of water to experimental values. We have equilibrated the system for a total of 40-ps. During the first two steps, the backbone heavy atoms of the β-helical (and also the α-helical if applicable) portions are positionally restrained using a harmonic potential. The hinge loops and the regions linking the β-helical and α-helical domains are allowed to freely move. To achieve the three different MD runs for the BPT and DSTP structures, we start with different initial temperatures that seed a different run through a different initial thermal distribution of atom velocities. Finally, we carry out a 1-ns production run at constant pressure and temperature with no positional restraints. For the high temperature (T=500K) simulations, the production runs are performed at constant volume with a reduced time step of integration to prevent any possible system blowup.

Hydrogen bonds are calculated based on the following criteria: *1)* direct hydrogen bonds in interface are counted with a donor-acceptor distance of 3.5 Å and a hydrogen-donor-acceptor angle of 60°, and *2)* water-bridged hydrogen bonding in interface is counted if a water molecule couples by criterion *1)* to an atom from each of two monomers.

D.L.C. thanks useful conversations with R. R. P. Singh and K. W. Plaxco; we also acknowledge fruitful discussions with P.G. Wolynes. This work was supported by the U.S. Army grant NP020132 and NSF Grants PHY0216576 and PHY0225630. Computing resources were supported by the San Diego Supercomputer Center and the NSF-sponsored Center for Theoretical Biological Physics.

REFERENCES

1. Prusiner, S. B. (2004) *Prion Biology and Diseases*, Cold Spring Harbor Press, Cold Spring Harbor, New York
2. Legname, G., Baskakov, I. V., Nguyen, H. O., Riesner, D., Cohen, F. E., DeArmond, S. J., and Prusiner, S. B. (2004) Synthetic mammalian prions. *Science* **305,** 673–676; Castilla, J., Sa'a, P., Hetz, C., Soto, C. (2005) In vitro generation of infectious scrapie prions. *Cell* **121,** 195–206
3. Wille, H., Michelitsch, M. D., Guenebaut, V., Supattone, S., Serban, A., Cohen, F. E., Agard, D. A., and Prusiner, S. B. (2002) Structural studies of the scrapie prion protein by electron crystallography. *Proc. Natl. Acad. Sci. USA* **99,** 3563–3568
4. Govaerts, C., Wille, H., Prusiner, S. B., and Cohen, F. E. (2004) Evidence for assembly of prions with left-handed β-helices into trimers. *Proc. Natl. Acad. Sci. USA* **101,** 8342–8347
5. Lindskog, S. (1997) Structure and mechanism of carbonic anhydrase. *Pharmacol. Ther.* **74,** 1–20
6. Stork, M., Giese, A., Kretzschmar, H. A., and Tavan, P. (2005) Molecular dynamics simulations indicate a possible role of parallel α-helices in seeded aggregation of poly-Gln. *Biophys. J.* **88,** 2442–2451
7. Guo, J. T., Wetzel, R., and Wu, Y. (2004) Molecular modeling of the core of Aâ amyloid fibrils. *Proteins* **57,** 357–364
8. Kishimoto, A., Hasegawa, K., Suzuki, H., Tauchi, H., Namba, K., and Yoshida, M. (2004) α-helix is a likely core structure of yeast prion Sup35 amyloid fibers. *Biochem. Biophys. Res. Commun.* **315,** 739–745
9. Pye, V. E., Tingey, A. P., Robson, R. L., and Moody, P. C. E. (2004) The structure and mechanism of serine acetyltransferase from *Escherichia coli*. *J. Biol. Chem.* **279,** 40729–40736
10. Lysek, D. A., and Wuthrich, K. (2004) Prion protein interaction with the C-Terminal SH3 domain of Grb2 studied using NMR and optical spectroscopy. *Biochemistry* **43,** 10393–10399
11. Bennett, M., Choe, S., and Eisenberg, D. (1994) Domain swapping: entangling alliances between proteins. *Proc. Natl. Acad. Sci. USA* **91,** 3127–3131
12. Bennett, M. J., Schlunegger, M. P., and Eisenberg, D. (1995) 3D domain swapping: a mechanism for oligomer assembly. *Protein Sci.* **4,** 2455–2468
13. Yang, S., Cho, S. S., Levy, Y., Cheung, M. S., Levine, H., Wolynes, P. G., and Onuchic, J. N. (2004) Domain swapping is a consequence of minimal frustration. *Proc. Natl. Acad. Sci. USA* **101,** 13786–13791
14. Bergdoll, M., Remy, M.-H., Cagnon, C., Masson, J.-M., and Dumas, P. (1997) Proline-dependent oligomerization with arm exchange. *Structure* **5,** 391–401
15. Rousseau, F., Schymkowitz, J. W. H., Wilkinson, H. R., and Itzhaki, L. S. (2001) Three-dimensional domain swapping in p13suc1 occurs in the unfolded state and is controlled by conserved proline residues. *Proc. Natl. Acad. Sci. USA* **98,** 5596–5601
16. Rousseau, F., Schymkowitz, J. W. H., and Itzhaki, L. S. (2003) The unfolding story of three-dimensional domain swapping. *Structure* **11,** 243–251
17. Sugimoto, T. (2003) Formation of monodispersed nano- and micro-particles controlled in size, shape, and internal structure. *Chem. Eng. Technol.* **26,** 313–321
18. Mobley, D. L., Cox, D. L., Singh, R. R. P., Kulkarni, R. V., and Slepoy, A. (2003) Simulations of oligomeric intermediates in prion diseases. *Biophys. J.* **85,** 2213–2223
19. Cohen, F. E., and Prusiner, S. B. (1998) Pathologic conformations of prion proteins. *Annu. Rev. Biochem.* **67,** 793–819
20. Knaus, K. J., Morillas, M., Swietnicki, W., Malone, M., Surewicz, W. K., and Yee, V. C. (2001) Crystal structure of the human prion protein reveals a mechanism for oligomerization. *Nat. Struct. Biol.* **8,** 770–774
21. Lee, S., and Eisenberg, D. (2003) Seeded conversion of recombinant prion protein to a disulfide-bonded oligomer by a reduction oxidation process. *Nat. Struct. Biol.* **10,** 725–730
22. Welker, E., Raymond, L. D., Scheraga, H. A., and Caughey, B. (2002) Intramolecular versus intermolecular disulfide bonds in prion proteins. *J. Biol. Chem.* **277,** 33477–33481
23. May, B.C.H., Govaerts, C., Prusiner, S.B., Cohen, F.E. (2004) Prions: so many fibers, so little infectivity. *Trends Biochem. Sci.* **29,** 162–165
24. Liu, Y., Gotte, G., Libonati, M., and Eisenberg, D. (2001) A domain-swapped RNase A dimer with implications for amyloid formation. *Nat. Struct. Biol.* **8,** 211–214
25. Janowski, R., Kozak, M., Jankowska, E., Grzonka, Z., Grubb, A., Abrahamson, M., and Jaskolski, M. (2001) Human cystatin C, an amyloidogenic protein, dimerizes through three-dimensional domain swapping. *Nat. Struct. Biol.* **8,** 316–320
26. Sinha, N., Tsai, C.-J., and Nussinov, R. (2001) A proposed structural model for amyloid fibril elongation: domain swapping forms an interdigitating β-structure polymer. *Protein Eng.* **14,** 93–103
27. Wetzel, R. (2002) Ideas of order for amyloid fibril structure. *Structure* **10,** 1031–1036
28. Pearlman, D. A., Case, D. A., Caldwell, J. W., Ross, W. R., Cheatham, T. E., III, DeBolt, S., Ferguson, D., Seibel, G., and Kollman, P. (1995) AMBER, a computer program for applying molecular mechanics, normal mode analysis, molecular dynamics and free energy calculations to elucidate the structures and energies of molecules. *Comp. Phys. Commun.* **91,** 1–41

Received for publication April 1, 2005.
Accepted for publication July 5, 2005.

APPENDIX C

A Mechanism for Copper Inhibition of Infectious Prion Conversion

Daniel L. Cox, Jianping Pan, and Rajiv R. P. Singh
Department of Physics, University of California at Davis, Davis, California 95616

ABSTRACT We employ ab initio electronic structure calculations to obtain two structural models for copper bound in the strongest binding site of the noninfectious form of the prion protein. The models are compatible with available experimental constraints from electron spin resonance data. The bending of the peptide backbone attendant with the copper binding is not compatible with the requisite straight β-strand backbone structure for the same sequence contained in two recently proposed models of the prion protein structure in its infectious form. We hypothesize that copper binding at this site is protective against conversion to the infectious form, discuss experimental data that appear to support and conflict with our hypothesis, and propose tests using recombinant prion protein, genetically modified cultured neurons, and transgenic mice.

Received for publication 24 February 2006 and in final form 17 April 2006.

Address reprint requests and inquiries to Daniel L. Cox, E-mail: cox@physics.ucdavis.edu.

The functional role of the normal cellular prion protein (PrP^C) may well be related to copper binding, potentially protecting against oxidative damage in the synaptic region by sequestering divalent copper (1). This suggestion is supported by data for transgenic knockout mice devoid of the gene for expressing PrP^C; these mice appear to suffer late stage oxidative degradation in the neuronal synaptic regions where surface bound prion protein is preferentially concentrated in wild-type mice (2,3). The strongest copper binding site is in the protein region that converts to β-sheet structure in the infectious (PrP^{Sc}) form (1). We use electronic structure calculations to study two possible geometries for the bound copper-PrP^C complex; we find that these geometries are incompatible with recently proposed models (4,5) for PrP^{Sc} oligomers, and we thus hypothesize a mechanism for inhibition of PrP^C-to-PrP^{Sc} conversion via copper binding.

Copper binds principally to mammalian PrP^C at octarepeat sites of highly conserved form (though not number) in a now well-understood pyramidal geometry with binding to the peptide backbone, histidine side chains, and axial waters (6). These octarepeats (residues 60–91 in humans) are not essential to PrP^{Sc}, which remains infectious even after proteinase exposure that leaves residues 92–230 intact. One strong copper binding site is present in the PrP^{Sc} core region, containing the sequence 92–96 GGGTH for humans. Electron spin resonance data suggest there is binding to the H96 (H95 in mice) side chain and the G94 amide group (1). It is not known whether the primary peptide coordination is to four nitrogens (NNNN) or to three nitrogens and an oxygen (NNON), although the former structure has been conjectured to be more likely (1).

We have studied this problem computationally with the SIESTA local orbital-based density functional theory code using conjugate gradient-based energy minimization to examine possible GGGTH-Cu(II) geometries (7,8). We have considered the NNNN structure and an NNON structure compatible with the ESR data (1) and our results are shown in the upper two panels of Fig. 1 for the mouse prion. We built initial candidate structures of the form Ac-Cu$(H_2O)_6$ (GGGTH)-NH_2 using ChemSite Pro (ChemSW, Fairfield, CA) and VMD (9). For each geometry, the lowest energy sampled provides our model bound copper-prion complex. We used double-zeta (DZ) basis sets for light atoms (H, C, N, O) and double-zeta polarized orbitals for copper. We used the Troullier-Martins norm-conserving pseudopotential. We employed the Perdew-Becke-Ernzerhof-based generalized gradient approximation exchange correlation energy functional. Our energy cutoff for matrix element integration was 120 Rydberg. All calculations were carried out in a periodic unit cell size: $30.7 \times 30.7 \times 30.7$ Å. Geometry minimization was carried out to a force tolerance of 32 pN.

Our main result is inferred from comparing the two possible GGGTH-Cu(II) geometries to recently proposed β-helical PrP^{Sc} trimer models (4,5). We see that the backbone bending induced by copper binding is not compatible with formation of β-strands in the left-handed helices. (It is unclear if another recently proposed model has the same characteristics (10).) Hence, copper in the nonoctarepeat sequence GGGTH can protect against PrP^C-to-PrP^{Sc} conversion; removal of this copper by pH reduction associated with synaptic fluctuations or endocytosis may be a key step in the conversion pathway. This picture is supported by the observation that only the GGTH sequence is required for binding, and eutherian prion sequences reveal high conservation of either GGTH or the very similar GGSH sequence in the converting region (11).

Removal of this copper by pH reduction may be a key step in the PrP^C-to-PrP^{Sc} conversion pathway because it is known that acidic conditions favor detachment of the copper (12). We note two routes for such a pH reduction with accompanying conversion of PrP^C. First, upon endocytosis into the cell, the pH is reduced. Assuming that some PrP^{Sc} is endo-

doi: 10.1529/biophysj.106.083642

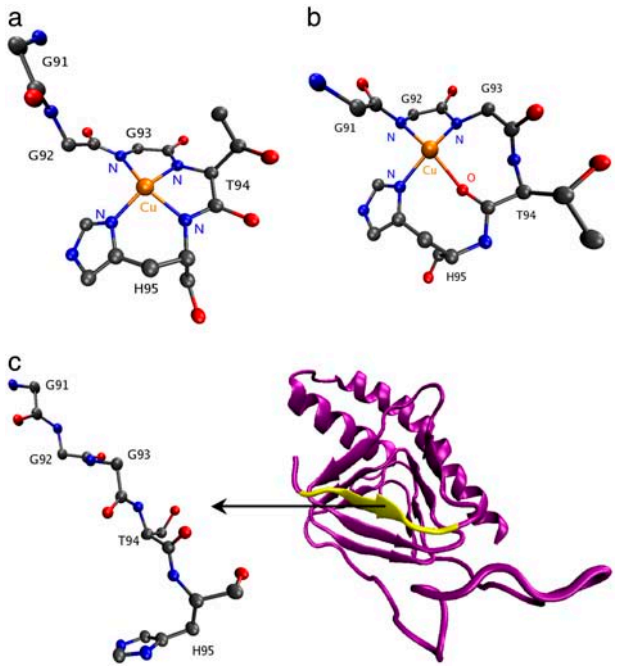

FIGURE 1 Potential copper binding motifs in the converting region of the normal (PrP^{C}) mouse prion protein, which are consistent with ESR data (1) are shown in panels *a* and *b*. The corresponding copper-free stretch of the left-handed β-helix model of the infectious (PrP^{Sc}) protein from Govaerts et al. (4) is shown in panel *c*.

cytosed as well as PrP^{C}, then conversion can take place within the endocytosed compartments after the copper is expelled. Second, given that PrP^{C} is preferentially concentrated near the synapse, then from signal bearing vesicles released near or at the synapse (13) can reduce the pH locally and facilitate copper expulsion.

Three experimental results support our proposed mechanism indirectly: 1), Postmortem studies show copper depletion in regions of infection, with 80–90% reduction of copper content in the corresponding prion proteins (14). This result is consistent with our mechanism, since this GGGTH binds Cu(II) first with potential cooperative enhancement of subsequent binding to other sites. If infection promotes removal of copper from this site, then it is more likely that copper will not be retained at the other sites assuming near-equilibrium conditions. 2), Copper uptake in infected cultured neurons is suppressed ~10-fold compared to control cells (15). Again, this is consistent with the hypothesis, although this requires an understanding of how the prion, which is easily shown to contain <1% of cellular copper, can shut down copper transport. 3), Copper in solution inhibits in vitro growth of amyloid fibrils (16,17). This is a more direct corollary to our hypothesized protective role of copper.

Other experiments provide mixed support for our mechanism. The copper chelator D-penicillamine inoculated in vivo delays disease onset, which is at apparent odds with our hypothesis (18). The chelator cuprizone, however, is known to induce a spongiosis (vacuolation of brain tissue) very similar to that of prion disease although it also induces demyelination of neurons and no transmissibility (19,20). Moreover, it is also known that copper confers proteinase resistance to the cellular prion protein in the weaker binding octarepeat regions (21). This is significant for two reasons. First, proteinase resistance is one of the generic hallmarks of the infectious form of the disease (although not all infectious prion protein is in fact proteinase resistant). Second, the octarepeat deletion does not remove infectivity from PrP^{Sc}. However, in transgenic mice without octarepeats, disease incubation upon direct intercerebral inoculation is slowed (22). Hence, these octarepeats are not necessary for disease, but i), they can impart structure in the presence of copper that confers proteinase resistance to the prion protein, and ii), their presence enhances disease incubation. Indeed, it is known that the octarepeat region adopts a unique structural motif when copper is bound (23). We can rationalize these data by assuming the following affinity ranking: cuprizone > nonoctarepeat site > D-PEN > octarepeat site. This ranking is plausible given the hexadentate chelation of cuprizone versus at most tetradentate coordination of D-PEN. With this assumption, D-PEN lifts the proteinase resistant structure associated with copper binding to octarepeats, and this slows conversion to the infectious form. These assumptions may be tested by performing competitive binding experiments in vitro with D-PEN (18), cuprizone (19), and the relevant copper binding segments of the prion protein. We note that the high affinity of cuprizone for divalent copper apparently leads to stripping of copper from other proteins so that the in vivo phenomena need not be limited to prions; if our assumptions are correct, these nonprion related effects must lead to more rapid degeneration of neurons than conversion to PrP^{Sc}.

To further test the mechanism, it is desirable to perform mutation studies on the stretch GGSH or GGTH. The key idea is to mutate out the H for, e.g., A,Y,G or other amino acids which should severely mitigate copper binding. We propose first that recombinant mutant PrP^{C} from residues 90–230 (with, e.g., H96A in the human form) be allowed to aggregate in copper-full and copper-free environments. Using the reduced length prion will avoid the confounding effects from the octarepeat regions discussed above. If the mechanism is correct, the fibril formation rate should be approximately the same as wild-type fibrils grown in copper-free solutions. Second, one can transfect cultured neurons with the mutated DNA construct and look for increased susceptibility to infection. Third, assuming positive results from the fibril growth and cultured neuron experiments, transgenic mice with the H95 mutated away; these mice should prove to have shorter incubation times for a given dose than wild-type mice. Finally, fibrillization experiments on recombinant marsupial PrP^{C} with and without copper should be informative since the H is replaced with Y24; our prediction based upon the present hypothesis would be that

the copper should have reduced inhibition of fibril formation relative to growth of recombinant human prion protein.

ACKNOWLEDGMENTS

We are grateful for conversations with D. Kleinfeld, G. S. Millhauser, and A. Nordlund, and for correspondence with E. D. Britt and J. Graves. We thank the CTBP for use of their computers. We are grateful to C. Govaerts for sharing the coordinate file for his model of Govaerts et al. (4).

We acknowledge the support of the U. S. Army (Congressionally Directed Medical Research Program, grant No. NP020132), National Science Foundation grant No. PHY0216576 for the Center for Theoretical Biological Physics of University of California at San Diego (D.L.C.), and the J. S. Guggenheim Memorial Foundation (D.L.C.).

REFERENCES and FOOTNOTES

1. Burns, C. S., E. Aronoff-Spencer, G. Legname, S. B. Prusiner, W. E. Antholine, G. J. Gerfen, J. Peisach, and G. L. Millhauser. 2003. Copper coordination in the full-length, recombinant prion protein. *Biochemistry*. 42:6794–6803.
2. Klamt, F., F. Dal-Pizzol, M. L. Conte da Frota Jr., R. Walz, M. E. Andrades, E. G. da Silva, R. R. Brentani, I. Izquierdo, and J. C. Fonsesca-Moreira. 2001. Imbalance of antioxidant defense in mice lacking cellular prion protein. *Free Radic. Biol. Med.* 30:1137–1144.
3. Sakudo, A., D-C. Lee, E. Yoshimura, S. Nagasaka, K. Nitta, K. Saeki, Y. Matsumoto, S. Lehmann, S. Itohara, S. Sakaguchi, and T. Onodera. 2004. Prion protein suppresses perturbation of cellular copper homeostasis under oxidative conditions. *Biochem. Biophys. Res. Commun.* 31: 850–855.
4. Govaerts, C., H. Wille, S. B. Prusiner, and F. E. Cohen. 2004. Evidence for assembly of prions with left-handed β-helices into trimers. *Proc. Natl. Acad. Sci. USA*. 90:8342–8347.
5. Yang, S., H. Levine, J. N. Onuchic, and D. L. Cox. 2005. Structure of infectious prions: stabilization by domain swapping. *FASEB. J.* 19: 1778–1782.
6. Burns, C. S., E. Aronoff-Spencer, C. M. Dunham, P. Lario, N. I. Avdievich, W. E. Antholine, M. M. Olmstead, A. Vrielink, G. J. Gerfen, J. Peisach, W. G. Scott, and G. L. Millhauser. 2002. Molecular features of the copper binding sites in the octarepeat domain of the prion protein. *Biochemistry*. 41:3991–4001.
7. Ordejon, P., E. Artacho, and J. M. Soler. 1996. Self-consistent order-N density-functional calculations for very large systems. *Phys. Rev. B*. 53:10441–10444.
8. Soler, J. M., E. Artacho, J. D. Gale, A. Garcia, J. Junquera, P. Ordejon, and D. Sanchez-Portal. 2002. The SIESTA method for ab initio order-N materials simulation. *J. Phys. Condens. Matter*. 14:2745–2779.
9. Humphrey, W., A. Dalke, and K. Schulten. 1996. VMD: visual molecular dynamics. *J. Mol. Graph.* 14:33–38.
10. DeMarcho, M. L., and V. Daggett. 2004. From conversion to aggregation: protofibril formation of the prion protein. *Proc. Nat. Acad. Sci. USA*. 101:2293–2298.
11. Horn, F., G. Vriend, and F. E. Cohen. 2001. Collecting and harvesting biological data: the GPCRDB and NucleaRDB databases. *Nucleic Acids Res.* 29:346–349 (and).
12. Aronoff-Spencer, E., C. S. Burns, N. I. Avdievich, G. J. Gerfen, J. Peisach, W. E. Antholine, H. L. Ball, F. E. Cohen, S. B. Prusiner, and G. L. Millhauser. 2000. Identification of the Cu2+ binding sites in the N-terminal domain of the prion protein by EPR and CD spectroscopy. *Biochemistry*. 39:13760–13771.
13. Chesler, M. 2003. Regulation and modulation of pH in the brain. *Physiol. Rev.* 83:1183–1221.
14. Wong, B.-S., S. G. Chen, M. Colucci, Z. Xie, T. Pan, T. Liu, R. Li, P. Gambetti, M-S. Sy, and D. R. Brown. 2001. Aberrant metal binding by prion protein in human prion disease. *J. Neurochem.* 78:1400–1408.
15. Rachidi, W., A. Mangé, A. Senator, P. Guiraud, J. Riondel, M. Benboubetra, A. Favier, and S. Lehmann. 2003. Prion infection impairs copper binding of cultured cells. *J. Biol. Chem.* 278:14595–14598.
16. Giese, A., J. Levin, U. Bertsch, and H. Kretzchmar. 2004. Effect of metal ions on de novo aggregation of full-length prion protein. *Biochem. Biophys. Res. Commun.* 320:1240–1246.
17. Bocharova, O. V., L. Breydo, V. V. Salnikov, and I. Baskakov. 2005. Copper(II) inhibits in vitro conversion of prion protein into amyloid fibrils. *Biochemistry*. 44:6776–6787.
18. Sigurdsson, E. M., D. R. Brown, M. A. Alim, H. Scholtzova, R. Carp, H. C. Meeker, F. Prelli, B. Frangione, and T. Wisniewski. 2003. Copper chelation delays the onset of prion disease. *J. Biol. Chem.* 278:46199–46202.
19. Pattison, I. H., and J. N. Jebbett. 1971. Histopathological similarities between scrapie and cuprizone toxicity in mice. *Nature*. 230:115–117.
20. Pattison, I. H., and J. N. Jebbett. 1973. Clinical and histological recovery from the scrapie like spongiform encephalopathy produced in mice by feeding them with cuprizone. *J. Pathol.* 109:245–250.
21. Quaglio, E., R. Chiesa, and D. A. Harris. 2001. Copper converts the cellular prion protein into a protease-resistant species that is distinct from the scrapie isoform. *J. Biol. Chem.* 276:11432–11438.
22. Supattapone, S., P. Bosque, T. Muramoto, H. Wille, C. Aagaard, D. Peretz, H. O. Nguyen, C. Heinrich, M. Torchia, J. Safar, F. E. Cohen, S. J. DeArmond, S. B. Prusiner, and M. Scott. 1999. Prion protein of 106 residues creates an artificial transmission barrier for prion replication in transgenic mice. *Cell*. 96:869–878.
23. Zahn, R. 2003. The octapeptide repeats in mammalian prion protein constitute a pH dependent folding and aggregation site. *J. Mol. Biol.* 334:477–488.
24. Premzl, M., M. Delbridge, J. E. Gready, P. Wilson, M. Johnson, J. Davis, E. Kuczek, and J. A. M. Graves. 2005. The prion protein gene: identifying regulatory signals using marsupial sequence. *Gene*. 349:121–134.

APPENDIX D

PHYSICAL REVIEW E **72**, 051915 (2005)

One-dimensional model of yeast prion aggregation

K. C. Kunes, D. L. Cox, and R. R. P. Singh
Department of Physics, University of California, Davis, California 95616, USA
(Received 3 May 2005; revised manuscript received 14 July 2005; published 9 November 2005)

Mammalian prion proteins (PrP) are of significant public health interest. Yeasts have proteins, which can undergo similar reconformation and aggregation processes to PrP, without posing a threat to the organism. These yeast "prions," such as SUP35, are simpler to experimentally study and model. Recent *in vitro* studies of the SUP35 protein found long aggregates, pure exponential growth of the misfolded form, and a lag time which depended weakly on the monomer concentration. To explain this data, we have extended a previous model of aggregation kinetics along with a stochastic approach. We assume reconformation only upon aggregation and include aggregate fissioning and an initial nucleation barrier. We find that for sufficiently small nucleation rates or seeding by a small number of preformed nuclei, the models achieve the requisite exponential growth, long aggregates, and a lag time which depends weakly on monomer concentration. The spread in aggregate sizes is well described by the Weibull distribution. All these properties point to the preeminent role of fissioning in the growth of misfolded proteins.

DOI: 10.1103/PhysRevE.72.051915 PACS number(s): 82.39.Fk

I. INTRODUCTION

Bovine spongiform encephalopathy (BSE) in cows, Scrapies in sheep, Creutzfeldt-Jakob Disease (CJD) and Kuru in humans are all diseases caused by a specific misfolded protein residing on neurons [1,2]. This prion protein (denoted PrP^c in its normal form and PrP^{sc} in its misfolded form) is present in all mammals and its full function, to date, is still unknown. A growing body of evidence strongly implies that this disease propagates not by nucleic acids, such as DNA or RNA, but by misfolded proteins (PrP^{sc}) [3,4]. In our current understanding of prion diseases, the autocatalytic misfolding of the prion proteins plays a central role. The misfolded form PrP^{sc} entices normal versions of the cellular prion protein (PrP^c) to change conformation to the misfolded or disease causing form. Although PrP^c and PrP^{sc} have the same amino acid sequence (230 amino acids or residues), PrP^{sc} has a higher beta sheet content than its normal form [1]. In humans, the disease is mostly sporadic, perhaps caused by a rare spontaneous misfold of the protein. But, infectious forms are also known to occur, such as in the case of new-variant CJD caused by eating BSE infected meat. In the latter case, infectious agents are presumably misfolded "seeds" that have entered the body from outside. Developing an understanding of the misfolding process should provide insights to prevention and/or cure of these diseases.

A class of proteins in yeast (SUP35) undergo a conformation change similar to the mammalian PrP. However, in case of yeast, this does not kill the organism. In fact, reconfigured, aggregated forms lead to a new phenotype [5]. Because they are not toxic, the misfolding is much easier to study for these proteins. Besides, it has been shown that aggregates produced *in vitro* can lead to the same phenotype, when added to a yeast cell [6–8]. Thus, it is possible to study the molecular aggregation processes for yeast prions in a test tube in tremendous detail, and a large quantity of experimental data is indeed available [9,10].

In this paper, we explore, using conventional kinetic as well as stochastic models, the aggregation dynamics for model yeast prions with a particular goal of explaining *in vitro* data [9,10] including (i) linear aggregates which grow by monomer addition, (ii) a modest concentration dependence of initial aggregate growth time varying roughly inversely as the square root of the monomer concentration, (iii) an observed distribution of aggregate sizes with a mode that is large ($10s-100s$ of monomers), and (iv) a sigmoidal growth that is nearly exponential. We extend the nucleation and fissioning model of Collins *et al.* [9,10] from a moments-only model to monitor individual polymer lengths and show that we can readily obtain the above listed features in the data. In particular, we argue against a model based upon rapid equilibration with micelles, which can also provide a weak concentration dependence to initial aggregation times [11,12], but not the exponential growth implied by including explicit fission of aggregates. The fission rate plays a central role in determining the time scales as well as the mean aggregate length. The range of aggregate sizes assumes a Weibull distribution, also well known from other processes where fissioning is important. Thus the agreement with experiments highlights the importance of fissioning in the growth dynamics.

We study our kinetics both with continuous time modeling and via the discrete time stochastic Gillespie algorithm. The motivation for applying the latter is to determine where stochastic effects from the relatively rare processes of large length polymer generation may be observable in experiment.

In considering the relevance of these studies to mammalian prions, there is an important caveat that arises from the fact that mammalian prions are glycosyl phosphatidylinositol (GPI) anchored on neuron cells and, thus, move in a two-dimensional plane and, hence, can lead to areal aggregates [13,14]. The aggregation and fissioning processes are likely to be very different there. Nevertheless, the dominance of fissioning can lead to long-time growth kinetics, which are in many ways closely related.

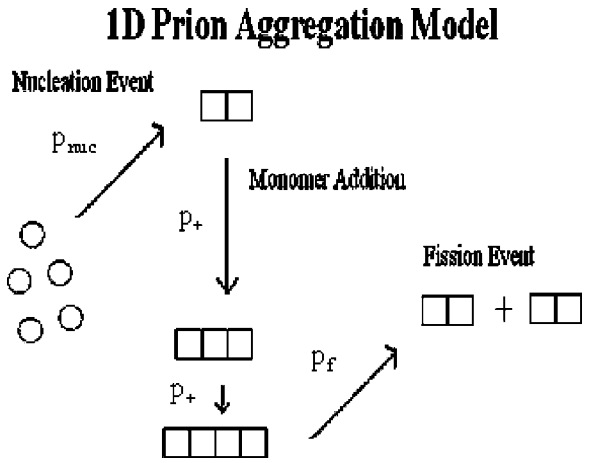

FIG. 1. Aggregation model where circles are normal proteins (psi^-) and squares are the misfolded type [PSI^+].

II. MODELS

We consider a one-dimensional aggregation model that includes a nucleation barrier, elongation by monomer addition, and fission (Fig. 1). The same kind of kinetics was considered by Collins *et al.* in the form of moments of the full polymer kinetic equations, but not in the explicit length resolved form considered here [9,10]. The assumption that monomer (rather than oligomer) addition dominates and the need for fission are underscored by the data we seek to describe on yeast prions [9,10]. We shall distinguish the model quantitatively from a nonfission based model later in the paper.

A nucleation event occurs very rarely and is composed of two normal [psi^-] proteins interacting in such a way that a misfold occurs and they bind together; this two prion aggregate is called a [PSI^+] dimer. The actual size of the nucleus is not a critical parameter in our model, as long as the nucleation process is much slower than aggregation. Once an aggregate has been created, it can elongate by monomer addition. Our model does not consider fusion between two oligomers. The rate of fissioning becomes important only when an oligomer of large enough size arises. After an oligomer has fissioned into smaller pieces, the individual pieces can grow and fission. When a fission leads to a monomeric product, we assume that it returns to the properly folded state. This process leads to a steady state distribution of oligomer sizes and a pure exponential growth. It continues until the monomer concentration begins to dwindle significantly.

We note that the lag time for the *in vitro* growth of yeast prion-like proteins is reproducible in experiments, and shows a weak dependence on monomer concentration. Hence, it is not likely that it can be associated with pure nucleation (at least at low initial monomer concentration), which being a rare event will lead to a distribution of time scales as well as a rather strong dependence on monomer concentration, depending on the size of the nucleus. We will assume that the lag time arises from the growth of misfolded material to an observability threshold. This assumption is valid if the nucleation time scales, which are long compared to other microscopic time scales, are still shorter than this latter time scale. It is also valid when a small number of nucleated seeds exist at the time of the preparation of the experimental samples. As shown elsewhere, a weak concentration dependence to lag time can derive from rapid equilibration of monomer concentration with nonfibrillar oligomers [11,12]; this model is not supported in the current context, and we shall discuss this later in this section.

A. Kinetic model

Our first approach is to use kinetic equations to describe the aggregation process [15,16]. In order to use the rate equations, one must assume a large number of monomers. The kinetic rate equations for our model are as follows

$$\frac{dn_1}{dt} = -2p_{nuc}n_1^2 - 2p_+n_1\sum_{i=2}^{N-1} n_i + 2p_f\sum_{i=2}^{N-1} n_i, \tag{1}$$

$$\frac{dn_2}{dt} = p_{nuc}n_1^2 - 2p_+n_1n_2 - p_fn_2 + 2p_f\sum_{i=3}^{N-1} n_i, \tag{2}$$

$$\frac{dn_k}{dt} = 2p_+n_{k-1}n_1 - 2p_+n_kn_1 - (k-1)p_fn_k + 2p_f\sum_{i=k+2}^{N-1} n_i, \tag{3}$$

$$\frac{dn_N}{dt} = 2p_+n_{N-1}n_1 - p_f(N-1)n_{N-1}, \tag{4}$$

where n_1 is the monomer concentration, n_k is the concentration of k-mers, and N is the longest oligomer kept in the calculation. The parameters p_{nuc}, p_+, and p_f can be adjusted to change the rate of nucleation, fusion, and fission, respectively. Since one of these parameters can be absorbed into the definition of the time t, we will set $p_+=1$. Furthermore, we will set the initial monomer concentration to unity. The equations listed above form a system of N-coupled differential equations which cannot be solved analytically because of the nonlinear terms.

An analytical solution is possible if n_1 can be assumed to be a constant and n_2 and higher are much, much smaller than the monomer concentration. Then the set of equations become linear and can be solved by several techniques, such as a Laplace transformation. This is not a bad approximation, for, as we will see, during much of the growth process the monomer concentration is nearly constant. Only at the end, the monomer concentration begins to dwindle and the amount of misfolded monomers saturates. It is useful to define the zeroth and first moments of the aggregate size distribution as

$$A = \sum_{i=2}^{N} n_i, \tag{5}$$

$$M = \sum_{i=2}^{N} i * n_i, \tag{6}$$

where A is the number of polymer aggregates and M is the total number of monomers in aggregate. Since the overall number of proteins is conserved, the rate of change of M is given by

$$\frac{dM}{dt} = -\frac{dn_1}{dt}, \tag{7}$$

whereas the rate of change of A is given (ignoring the cutoff N) by the equation

$$\frac{dA}{dt} = p_{nuc} n_1^2 - p_f n_2 + p_f \sum_{i=3} (i-3) n_i. \tag{8}$$

If we ignore the terms depending on n_2 and assume n_1 is a constant, we get two linear coupled equations,

$$\frac{dA}{dt} = \text{const} + p_f M - 3 p_f A, \tag{9}$$

$$\frac{dM}{dt} = \text{const} + (2p_+ n_1 - 2p_f) A. \tag{10}$$

We set $p_+ = 1$ to set the unit of time. Anticipating $M \gg A$, which means that the mean aggregate size is much bigger than unity. The above equations mean that the M and A both grow exponentially as $e^{\lambda t}$, with λ given by

$$\lambda = \sqrt{2p_f(n_1 - p_f)} \approx \sqrt{2p_f n_1}. \tag{11}$$

During the exponential growth, the mean aggregate size is given by

$$\bar{L} = \frac{M}{A} = \sqrt{\frac{2n_1}{p_f}}. \tag{12}$$

If we further assume that the lag time is given by the time it takes for the misfolded proteins to reach a detectable threshold M_f, then the lag time is given by

$$t_{lag} \sim \frac{\ln \dfrac{M_f}{C(n_1)^2}}{\sqrt{2p_f n_1}}, \tag{13}$$

where C is a constant and the n_1 dependence inside the logarithm comes from the prefactors. We will see that these results are confirmed by a complete numerical integration of the differential equations. Thus, this model demonstrates the requisite t-lag dependence seen in the experimental data, namely the inverse square root dependence on the monomer concentration, up to logarithms, shown in Fig. 2. We note that the fit in Fig. 2 is not sensitive to the logarithmic terms.

Kinetic model results

A numerical integration approach was used to study the full set of equations. We used the fourth order Runge-Kutta algorithm for solving differential equations and to obtain length distributions and growth curves for the system.

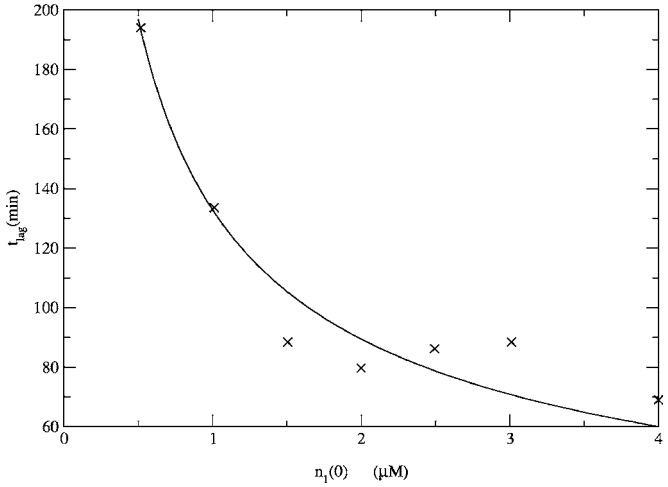

FIG. 2. Lag time (t_{lag}) vs initial monomer concentration $[n_1(0)]$. The crosses are data from Collins *et al.* in Ref. [9]. The continous curve is a fit to the equation $t_{lag} = a_0 [n_1(0)]^{-1/2} \log a_1/n_1(0)$, with $a_0 = 9.22\ min * (\mu M)^{1/2}$ and $a_1 = 1.80 \times 10^6 \mu M$, following Eq. (13).

In Fig. 3, we show plots of $\log(M)$ as a function of time. We have chosen a set of parameters yielding mean lengths in the $10s - 100s$ and displaying manifest exponential growth in $M(t)$ vs t plots. It is evident that there is a regime where $\log(M)$ varies linearly with time, implying a pure exponential growth. This region of exponential growth is not limited to just a few chosen parameter values, but can be achieved over a wide range of p_f values. In Fig. 3, we plot the total number in aggregate vs time, now on a linear scale. The sigmoidal growth is now evident as the exponential increase tapers off when the monomers begin to deplete. This is also consistent with the experimental results [9].

As discussed earlier, the mean length of the aggregates has a simple inverse square-root dependence on the rate of fission. Thus by tuning the rate of fission, it is possible to obtain mean aggregate lengths (see Fig. 4), which appear

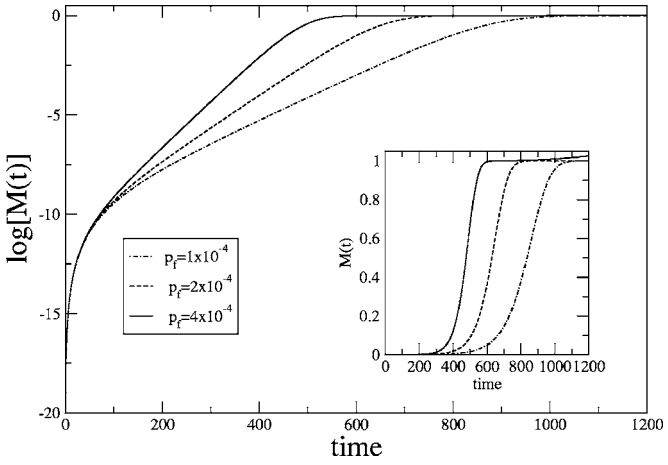

FIG. 3. Log$[M(t)]$ vs time, with parameter values $n_1(0) = 1$, $p_+ = 1$, $p_{nuc} = 10^{-8}$. The linear regions illustrate regions of pure exponential growth. $M(t)$ vs time illustrating sigmoidal growth is shown in the inset. Note that time is in units of $1/[n_1(0)p_+]$.

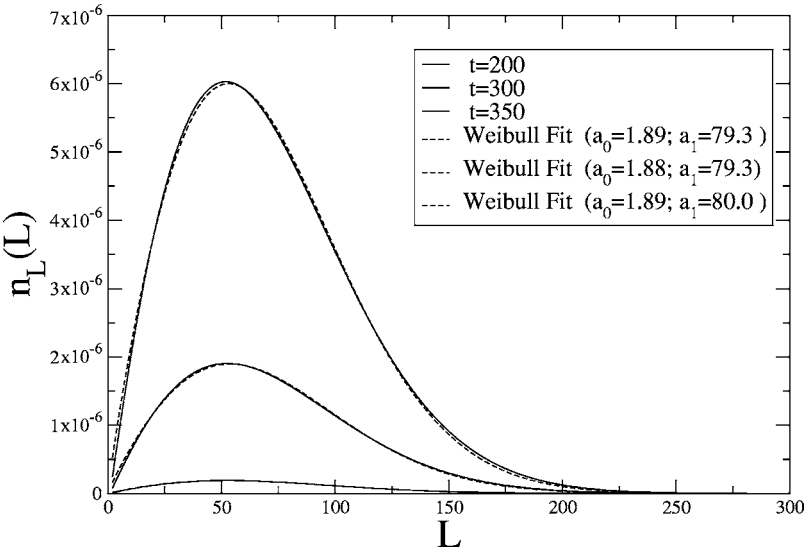

FIG. 4. Length distribution, n_l vs length L, from the kinetic equations during the exponential growth phase, compared with the Weibull distribution, Eq. (14).

qualitatively consistent with those observed experimentally displaying lengths in the tens of hundreds (see especially slide 9 at Ref. [10]). In Fig. 5, this mean length is plotted vs time for a different fission rate p_f. We see that the mean aggregate length is constant during the exponential growth. In Fig. 6, we show the variation of the exponential growth rate with p_f compared with the analytic calculations. One can see that they agree closely. Note also that p_f values of order 10^{-4} will give the lengths seen *in vitro*.

We can also determine the distribution of aggregate sizes in our calculations. The concentration of aggregates of different sizes relative to the initial concentration of monomers are shown in Fig. 4 for a given value of the fission parameter ($p_f=4\times10^{-4}$) at three different times during the exponential growth phase of the simulation. Clearly, the distribution is fairly stable during the exponential growth phase, further strengthening the argument for a simple steady state. These length distributions are well fitted by a Weibull distribution given by the relation,

$$f(x)=\frac{a_0}{a_1}\left(\frac{x}{a_1}\right)^{a_0-1}\exp\left[-\left(\frac{x}{a_1}\right)^{a_0}\right]. \tag{14}$$

Apart from an overall normalization, the two key parameters of the distribution are the mean a_1 and the power law at small x set by a_0-1. This distribution is found to be ubiquitous in nature [17]. For example, a dropped piece of coal will have shattered pieces that follow an asymmetrical distribution with more pieces on the smaller end. Our model follows a similar idea (i.e., taking a larger length and shattering it into smaller lengths) and a similar distribution. In our simulations, the quantity a_0 is close to 2 for a range of parameters studied. During subsequent times, the peak of this curve shifts to the left as saturation occurs and the only process left is to fission. (The shift in peak at later times are not shown here.)

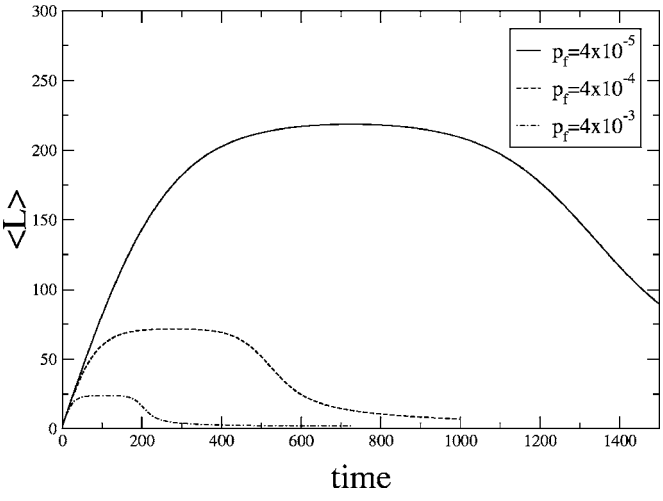

FIG. 5. Mean length vs time for different p_f; $n_1(0)=1$, $p_+=1$, $p_{nuc}=10^{-8}$. The plateau corresponds to the constant mean length during the exponential growth phase. Note that time is in units of $1/[n_1(0)p_+]$.

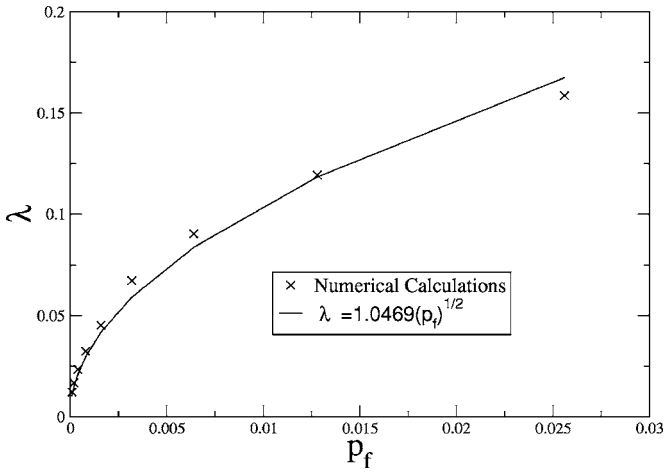

FIG. 6. Exponential growth rate λ vs p_f compared with simple square-root dependence predicted by Eq. (11) for different parameter values, $n_1(0)=1$, $p_+=1$, $p_{nuc}=10^{-8}$.

B. Comparison to nonfissioning micelle model

The coupling of the observation of weak concentration dependence with exponential growth strongly supports a model dominated by fissioning of aggregates constructed by monomer addition. Indeed, centrifugation studies confirm that monomers are the dominant species in the *in vitro* medium, and examination of the aggregation kinetics suggests a critical nucleus of small size [9].

It is thus important to contrast with other models for which a weak concentration dependence can be derived. Notably, the work of Lomakin *et al.* [11,12] considers kinetics with monomer growth of polymers as well as micellar oligomers composed of $\mathcal{M}$ monomers of concentration $n_{\mathcal{M}}$ which may or may not be off pathway. This model may be of relevance to other *in vitro* studies of yeast prion aggregation [18] for which there is evidence of oligomer formation and growth and a weak concentration dependence to the lag time. If the oligomers are off pathway, then assuming an equilibration with monomers leads to a buffering of the monomer concentration assuming an initially high input concentration and sufficiently rapid equilibration. There is a crossover or critical concentration n^* for this dictated by the equilibrium constant $K_{\mathcal{M}}$ between monomers and micelles ($K_{\mathcal{M}}=n_{\mathcal{M}}/n_1^{\mathcal{M}}$) given by

$$n^* = (\mathcal{M}K_{\mathcal{M}})^{1/1-\mathcal{M}}. \tag{15}$$

Lomakin *et al.* argue that for a total equilibrated protein concentration n_T obtained prior to fibril growth,

$$n_T = n_1 + \mathcal{M}n_{\mathcal{M}} \tag{16}$$

$$= n_1 + n^*\left(\frac{n_1}{n^*}\right)^{\mathcal{M}}. \tag{17}$$

From these equations, it is clear that there is an approximate two-state behavior provided $\mathcal{M} \gg 1$. For $n_T \ll n^*$, then $n_T \approx n_1$ and aggregation kinetics can be strongly concentration dependent. However, for $n_T \geqslant n^*$, then $n_1 \approx n^*$, that is, the micelles buffer the monomer concentration. This would lead to a weak dependence of fibrillar growth upon subsequent increase of initial monomer concentrations.

There are two routes by which this model can be applied to the data of Collins *et al.* [9,10]. First, if the fibrils are formed from monomer addition to the micelles without resulting fission of fibrils, then one will expect a quadratic growth in time [19,20] to the total number of aggregated proteins, namely

$$M(t) \approx \frac{1}{2}p_+^2 n_1^2 n_{\mathcal{M}} t^2, \tag{18}$$

$$\approx \frac{1}{2\mathcal{M}}p_+^2 n_1^{2+\mathcal{M}} (n^*)^{1-\mathcal{M}} n_{\mathcal{M}} t^2, \tag{19}$$

which is very weakly dependent upon $n_1(0)$ provided $n_1(0) \approx n_T \geqslant n^*$, but varies strongly as $n_1(0)^{2+\mathcal{M}}$ in the opposite limit. Solving for where $M(t_{lag})=M_c$ characteristic of the observability threshold yields

$$t_{lag} = \frac{1}{p_+ n_1}\sqrt{\frac{2M_c (n^*)^{\mathcal{M}-1}}{(n_1)^{\mathcal{M}}}}. \tag{20}$$

For $n_1(0) \ll n^*$, t_{lag} varies as $n_1(0)^{-(1+\mathcal{M}/2)}$, at odds with experiment [9], while for $n_1(0) \geqslant n^*$ and $\mathcal{M} \gg 1$, t_{lag} is approximately independent of $n_1(0)$ [it will decrease weakly with increasing $n_1(0)$].

Second, if the micelles are off pathway, then their principal impact on the fibrillar aggregation is on buffering. Assuming a critical fibrillar nucleus of length p, which equilibrates with the monomers via a constant $K_p=n_p/n_1^p$, the same considerations of aggregation kinetics as in the preceding paragraph give a lag time given by

$$t_{lag} = \frac{1}{p_+ n_1}\sqrt{\frac{2M_c}{K_p (n_1)^p}}. \tag{21}$$

For $n_1(0) \ll n^*$, this varies as $n_1(0)^{-(1+p/2)}$ is at odds with Collins *et al.* [9], while it is approximately independent of $n_1(0)$ for $n_1(0) \geqslant n^*$ and $p \gg 2$. For small nuclei ($p \simeq 2$–5, say), the dependence can be relatively strong on $n_1(0)$ even in this limit.

Hence, via either on-pathway or off-pathway micelles, in this model there is a route to weak dependence of lag time (defined as the threshold for observation) upon initial monomer concentration requiring $n_1(0) \geqslant n^*$ and $\mathcal{M}, p \gg 1$. However, there are several problems in connecting this to the experiments of Collins *et al.* First, exponential growth is unambiguously observed, indicating that fission of fibrils occurs. The micelle model of this subsection has no fission. This highlights the important role of fission for the prion phenomenon. Second, in these experiments, the starting solution contains almost entirely monomers and not micelles. This implies that even if micelles form, one is always in the limit of $n_1(0) \ll n^*$, leading to strong concentration dependence. Third, the width of the fibrils obtained in this experiment is apparently monomeric, which is not readily compatible with growth by monomer addition to micelles, and rather must be obtained by addition to a critical fibril nucleus. The data suggest that this critical fibril nucleus is of length $p \leqslant 6$, not consistent with the assumption $p \gg 1$.

Hence, we do not believe that the micelle based model can explain the data of Collins *et al.* [9,10].

C. Stochastic model

In this section, we develop a stochastic treatment of the model, similar to a model proposed by Pöschel *et al.* [21]. Our main motivation is to be able to treat species with small numbers, in which case the continuous deterministic approach will break down. As we will see, the stochastic approach largely agrees with the deterministic model for the parameter values considered here for aggregate quantities [e.g., $M(t)$]. However, for distributions there can be substantial stochastic noise at short times. Another advantage of the stochastic approach is that it can be readily extended to study

TABLE I. Propensities of stochastic processes.

Nucleation propensity	Fusion propensity for monomer addition		Higher order fusion term	Fission propensity for monomer		Higher order fission term
	Chain length 2	Chain length 3		Chain length 2	Chain length 3	
$g_{nuc}N_1(n_1-1)$	$2g_+N_1N_2$	$2g_+N_1N_3$	…	g_fN_2	$2g_fN_3$	…

two-dimensional aggregates as well as the problem of multiple prion "strains," in which case the treatment of a small number of heteroaggregates would be important to model the extent to which strains breed true.

The Gillespie algorithm provides an exact way to treat the stochastic problem of chemical reactions [22]. In our case, the polymers of different lengths are the different chemical species. The processes of nucleation, monomer addition, and fission are assumed to be stochastic. In other words, the number of polymers of different length at time t, only define the propensities (or normalized probability) for the different reactions to happen at that time. Once a reaction takes place, the number of polymers is altered and the propensities are changed. The Gillespie algorithm is a Monte Carlo treatment that deals with the stochastic process by using a pair of random numbers at each step, one to decide which event will occur next and another to decide how long will it be until the next event takes place. This process can be repeated to follow the dynamical behavior of the system.

Our model has the corresponding propensities

$$g_{nuc}N_1(N_1-1)+2g_+N_1\sum_{i=2}^{\infty}N_i+g_f\sum_{i=2}^{\infty}(i-1)N_i, \qquad (22)$$

where g_{nuc}, g_+, and g_f are, respectively, the nucleation, fusion, and fission parameters in the stochastic model. In our model, each propensity was assigned a bin in an array. A random number generator decides which bin is selected.

Table I illustrates physically the propensities at a given time. A normalized random number generator selects which element in the array will occur and the time it took to create that event. After an event occurs, the corresponding propensities are updated and the process is repeated.

In order to compare the results achieved from the continuous to stochastic model, a mapping of the Gillespie parameters to the kinetic parameters is required. For this, we need to develop an approximate equation satisfied by the monomer concentration in the stochastic simulations and compare it with the rate equations. In the stochastic case, one has a master equation that relates the probability distribution associated with a different number of polymers at time $t+dt$ to those at time t. We will make a mean-field approximation for different kind of k-mers, namely $\langle N_i * N_k\rangle = \langle N_i\rangle * \langle N_k\rangle$. Thus, we can consider the approximate master equation, which only tracks changes in the monomer number. We arrive at the equation,

$$\begin{aligned}P_1(N_1,t+dt) = P_1(N_1,t)\Bigg[1-g_{nuc}N_1(n_1-1)dt-g_+N_1\sum_{i=2}^{\infty}N_i dt \\ -2g_f\sum_{i=2}^{\infty}N_i dt\Bigg]+2P_1(N_1-1,t)g_f\sum_{i=3}^{\infty}N_i dt \\ +P_1(N_1-2,t)g_fN_2dt+P_1(N_1+1,t)g_+N_1 \\ \times\sum_{i=2}^{\infty}N_i dt+P_1(N_1+2,t)g_{nuc}N_1(N_1-1)dt,\end{aligned} \qquad (23)$$

where N_1 is the number of monomers, $P_1(N_1,t+dt)$ is the probability to have N_1 monomers at a later time $t+dt$. $P_1(N_1,t)$ is the probability to have N_1 monomers at time t. It is multiplied by the probability that no reaction occurs in time dt that changes N_1. The rest of the terms represent the probability to have a different number of monomers at time t but then a reaction happens in time dt leading to N_1 monomers at time $t+dt$.

Now using the definition of the derivative, one can rearrange the equation and multiply both sides by N_1 to get the average rate of change of N_1. After shifting some indices to get every probability to have the form $P_1(N_1,t)$ and using the appropriate volume element (denoted by V) to normalize the counts to a concentration, one arrives at the equation for the mean number of monomers,

$$\frac{1}{Vg_+}\frac{dn_1}{dt_{gil}} = -2g_{nuc}n_1^2-2n_1\sum_{i=2}^{\infty}n_i+2\frac{g_f}{V}\sum_{i=2}^{\infty}n_i. \qquad (24)$$

By comparing with the rate equations discussed before, we obtain the parameter mapping

$$p_+ = 1, \qquad (25)$$

$$p_{nuc} = g_{nuc}, \qquad (26)$$

$$p_f = \frac{g_f}{V}, \qquad (27)$$

$$t_{kinetic} = g_+Vt_{gillespie}. \qquad (28)$$

Results stochastic approach

After achieving the parameter mapping, we studied the stochastic models with 10^6 initial monomers. The numerical results are shown in the next few figures. In Fig. 7, the growth of the aggregate material is shown on a logarithmic

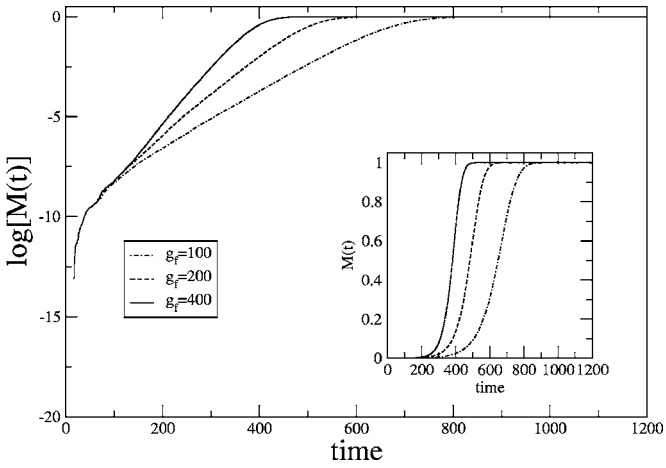

FIG. 7. Log$[M(t)]$ and $M(t)$, shown in the inset, vs time obtained by the Gillespie algorithm with $N_1(0)=10^6$, $g_+=1$, $g_{nuc}=10^{-8}$ for different fission rate g_f. Note that time is in units of $1/g_+$.

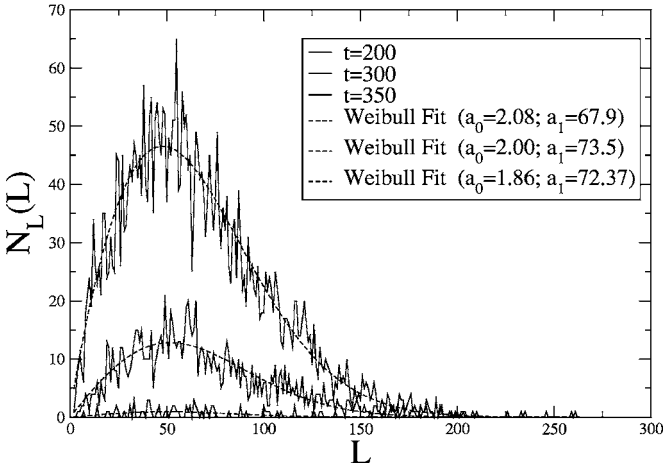

FIG. 9. Length distributions at different times during the exponential growth phase obtained by the Gillespie algorithm for $g_f=400$ and fitted by the Weibull distribution.

and on a linear scale. It is evident that they are in excellent agreement with the corresponding calculations for the kinetic model. In Fig. 8, we show plots of the mean length as a function of time, and in Fig. 9, the corresponding distribution of length scales during the exponential growth phase. It is again evident that there is a steady state during the exponential growth and the mean lengths reach a plateau value. The stochastic effects are much larger in the distribution and in the mean length, but the overall results agree well with the kinetic model. The fits to the Weibull distribution are again good with comparable parameters. The differences between the kinetic and stochastic Weibull parameters (a_0 and a_1) are less than 10%. This shows that for 10^6 monomers and for mean aggregate lengths up to a few hundred, the dominant species still occur in large enough numbers so that stochastic effects do not change the results in a significant way.

III. DISCUSSION

In this paper, we have used a deterministic kinetic and a stochastic Monte Carlo approach to model the dynamics of yeast prion growth. For the parameters relevant to *in vitro* experiments, where mean aggregate size is of order 100*s* of monomers, and the number of monomers is larger than 10^6, the two approaches agree well with each other, showing that stochastic effects are not dominant. The studies confirm that the key experimental features of the growth of yeast prions can be well captured by these nucleation-growth-fissioning models. They lead to an exponential and/or sigmoidal growth, an inverse square-root dependence of the lag time on the monomer concentration, and aggregate sizes that depend on the rate of fission. We predict that the aggregate size distributions should be Weibullian, reflecting the importance of fissioning in the growth process. We also predict, for sufficiently large times, that the steady state aggregate length will drop as fissioning converts large aggregates to those of minimal size. We have argued that models in which monomers equilibrate with micelles but do not fission [11,12], which are capable of producing lag times having a weak concentration dependence for a sufficiently high initial monomer concentration, are in fact not appropriate for the data of Collins *et al.* [9,10].

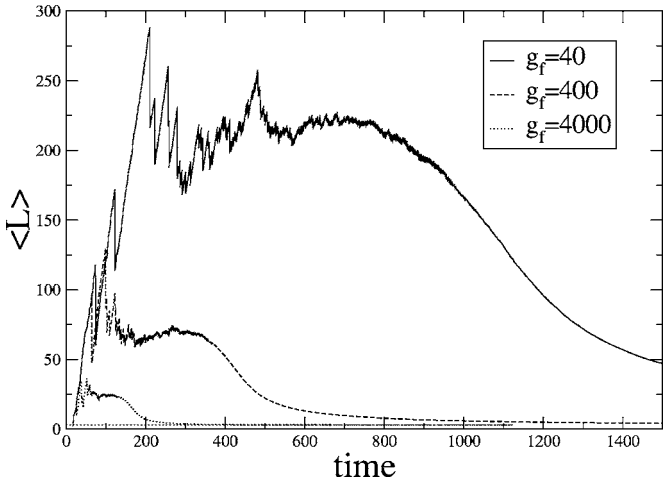

FIG. 8. Mean length vs time in units of $1/g_+$ for different fission rates g_f obtained by the Gillespie algorithm. The parameter values are $N_1(0)=10^6$, $g_+=1$, $g_{nuc}=10^{-8}$.

We note that the *in vitro* aggregation work of Serio *et al.* [18] appears to come to different conclusions than that of Collins *et al.* [9] and may be ripe for a discussion in terms of the micelle models. We do not understand the discrepancies between these two sets of experiments.

We note that the results on yeast prions discussed here and recent work on mammalian prions stripped of their GPI membrane anchors [23,24] suggest that a fundamentally different mechanism for fission is at play for the latter proteins *vis-à-vis* yeast. In the recent experiments, transgenic mice expressing the cellular prion protein without the residues necessary for the GPI anchor are exposed to anchorless infectious prions; in time course experiments, prion aggregates are produced which retain infectivity. However, the infected mice with anchorless PrP^C do not show clinical symptoms. Moreover, the time course data {see Fig. 1(c) of Chesebro *et al.* [24]} show two remarkable characteristics: (i) they are nonsigmoidal in shape, with the infectious prion content at long times significantly exceeding that of infected wild type

mice at death, (ii) the time scales to reach the levels of infectivity characteristic of wild type mice at the corresponding infectious dose are quite long. Indeed, the time course data can be fit roughly by a quadratic in time curve characteristic of nonfissioning aggregation to an initial concentration of infectious seeds. Evidently, the binding of cellular mammalian prions to the membrane is critical to the fissioning process, while for yeast prions fissioning of aggregates *in vitro* is observed [9].

In the future, we hope to extend this model to study yeast prion strains, where we expect the stochastic treatment to be the key to dealing with rare heteroaggregates. An understanding of this process should lead to insights into the important problem of strain dynamics in mammalian prions.

ACKNOWLEDGMENTS

We acknowledge the support of the U.S. Army Congressionally Mandated Biomedical Research Fund (Grant No. NP020132) and acknowledge the support of the NSF sponsored Center for Theoretical Biological Physics (NSF Grant Nos. PHY0216576 and 0225630). D.L.C. acknowledges the support of the J. S. Guggenheim Memorial Foundation.

[1] For a general introduction to prion biology, see S. B. Prusiner, *Prion Biology and Diseases*, 2nd ed. (C.S.H.L. Press, Cold Spring Harbor, NY, 2004).
[2] A. Aguzzi and M. Polymendiou, Cell **116**, 313 (2004).
[3] S. B. Prusiner, Science **216**, 136 (1982).
[4] G. Legname, I. Baskakov, H. Nguyen, D. Riesner, F. Cohen, S. DeArmond, and S. Pruisner, Science **305**, 673 (2004).
[5] R. B. Wickner, Science **264**, 566 (1994).
[6] H. E. Sparrer, A. Santosh, F. C. Szoka, Jr., and J. S. Weissman, Science **289**, 595 (2000).
[7] C. Y. King and R. Diaz-Avalos, Nature (London) **428**, 319 (2004).
[8] M. Tanaka, P. Chien, L. Z. Osherovich, and J. S. Weissman, Nature (London) **428**, 323 (2004).
[9] S. R. Collins, A. Douglass, R. Vale, and J. S. Weissman, PLoS Biol. **2**, 10 (2004).
[10] http://online.itp.ucsb.edu/online/bionet03/collins/
[11] A. Lomakin, D. S. Chung, G. B. Benedek, D. A. Kirschner, and D. A. Teplow, Proc. Natl. Acad. Sci. U.S.A. **93**, 1125 (1996).
[12] A. Lomakin, D. B. Teplow, D. A. Kirschner, and G. B. Benedek, Proc. Natl. Acad. Sci. U.S.A. **94**, 7942 (1997).
[13] A. Slepoy, R. R. P. Singh, F. Pazmandi, R. V. Kulkarni, and D. L. Cox, Phys. Rev. Lett. **87**, 058101 (2001).
[14] Holger Wille, Melissa D. Michelitsch, Vincent Guénebaut, Surachai Supattapone, Ana Serban, Fred E. Cohen, David A. Agard, and Stanley B. Prusiner, Proc. Natl. Acad. Sci. U.S.A. **99**, 3563 (2002).
[15] D. Hall and H. Edskes, J. Mol. Biol. **336**, 775 (2004).
[16] J. Masel, V. A. A. Jansen, and M. A. Nowak, Biophys. Chem. **77**, 139 (1999).
[17] W. Brown and K. Wohletz, J. Appl. Phys. **78**, 2758 (1995).
[18] T. R. Serio, A. G. Cashikar, A. S. Kowal, G. J. Sawicki, J. J. Moslehi, L. Serpell, M. F. Arnsdorf, and S. L. Lindquist, Science **289**, 1317 (2000).
[19] F. Ferrone, Methods Enzymol. **309**, 256 (1999).
[20] S. Chen, F. A. Ferrone, and R. Wetzel, Proc. Natl. Acad. Sci. U.S.A. **99**, 11884 (2002).
[21] T. Pöschel, N. V. Brilliantov, and C. Frömmel, Biophys. J. **85**, 3460 (2003).
[22] D. Gillespie, J. Comput. Phys. **22**, 403 (1976).
[23] P. Chien and J. Weissman, Nature (London) **410**, 223 (2001).
[24] B. Chesebro, M. Trifilo, R. Race, K. Meade-White, C. Teng, R. LaCasse, L. Raymond, C. Favara, G. Baron, S. Priola, B. Caughey, E. Masliah, and M. Oldstone, Science **308**, 1435 (2005).

APPENDIX E

Biophysical Journal: Biophysical Letters

Prion Disease: Exponential Growth Requires Membrane Binding

Daniel L. Cox,*† Rajiv R. P. Sing,* and Sichun Yang†
*Department of Physics, University of California, Davis, California 95616; and †Center for Theoretical Biological Physics, University of California, San Diego, La Jolla, California 92093

ABSTRACT A hallmark feature of prions, whether in mammals or yeast and fungi, is exponential growth associated with fission or autocatalysis of protein aggregates. We have employed a rigorous kinetic analysis to recent data from transgenic mice lacking a glycosylphosphatidylinositol membrane anchor to the normal cellular PrP^C protein, which show that toxicity requires the membrane binding. We find as well that the membrane is necessary for exponential growth of prion aggregates; without it, the kinetics is simply the quadratic-in-time growth characteristic of linear elongation as observed frequently in in vitro amyloid growth experiments with other proteins. This requires both: i), a substantial intercellular concentration of anchorless PrP^C, and ii), a concentration of small scrapies seeding aggregates from the inoculum, which remains relatively constant with time and exceeds the concentration of large polymeric aggregates. We also can explain via this analysis why mice heterozygous for the anchor-full/anchor-free PrP^C proteins have more rapid incubation than mice heterozygous for anchor-full/null PrP^C, and contrast the mammalian membrane associated fission or autocatalysis with the membrane free fission of yeast and fungal prions.

Received for publication 19 January 2006 and in final form 17 March 2006.

Address reprint requests and inquiries to D. L. Cox, E-mail: cox@physics.ucdavis.edu.

Prions are distinguished from other amyloid diseases both by their infectious character and the observed exponential growth of infectious material in vivo (1). There is a correspondence to this of prion-like proteins in yeast and fungi, for which spontaneous fission is reported in vitro (2). In fact, it has been argued that the replication necessary for infection in mammals and non-Mendelian inheritance in yeast/fungi requires the fission or autocatalysis that drives the exponential growth (1). It has been established for yeast prions that additional chaperone proteins most likely facilitate the fission of aggregates in living cells (1). It is an open question what mechanism drives the exponential growth in mammals. Here we show by a rigorous kinetic analysis of recent disease time course data that the exponential growth is tied to membrane anchoring of the prion protein, suggesting that either mechanical fission of areal prion aggregates or oligomeric autocatalysis of membrane bound prions explain the observed behavior.

Chesebro et al. (3) recently studied transgenic (Tg) mice lacking a GPI membrane anchor to the normal cellular PrP^C protein and discovered that these mice grew infectious prions without suffering neuronal death. We denote these anchorless cellular prions as $PrP^C_{Tg,}$ and anchor-full wild-type (WT) cellular prions by PrP^C_{WT}. When inoculated with infectious scrapies prions (PrP^{Sc}) at a dose that induces clinical symptoms within 140–160 days for WT mice, the Tg mice were symptomless up to 400–600 days, even though proteinase resistant PrP-res, an indicator of infectivity, accumulated and surpassed the maximal WT levels.

In Fig. 1 the Tg mice PrP-res concentration (*crosses*) of Chesebro et al. (3) are plotted versus the square of time, together with a linear regression fit (*line*) with a high regression coefficient ($R = 0.97$). This time dependence is consistent with short time kinetics described by linear polymer elongation via monomer addition without fission or autocatalysis (4), illustrated schematically in Fig. 2. Assuming the PrP-res concentration to be a proxy for the total protein content in aggregate, simple kinetic arguments predict a behavior, before monomer depletion and seed nucleus depletion, of

$$[\text{PrP-res}](t) \propto (1/2)(p_+[\text{PrP}^C_{Tg}])^2[\text{PrP}^{Sc}_n]\,t^2, \qquad (1)$$

with $p_+[\text{PrP}^C_{Tg}]$ the elongation rate at intercellular monomer Tg prion concentration $[\text{PrP}^C_{Tg}]$, and $[\text{PrP}^{Sc}_n]$ is the intercellular concentration of seeding nuclei from inoculated scrapies protein after initial hydrodynamic clearance. The validity of Eq. 1 at long times suggests that: i), there is a substantial homeostatic concentration of intercellular PrP^C_{Tg} presumably due to slow clearance, and ii), $[\text{PrP}^{Sc}_n]$ is hardly changed implying either that only a small fraction of seeds grow into large polymers or $[\text{PrP}^{Sc}_n]$ is maintained by steady proteolytic degradation of large remnant aggregates from the dose. Given a similar de novo production rate of PrP^C_{WT} in inoculated WT mice, we speculate that the associated saturation of [PrP-res] arises from loss of PrP^C_{WT} after cell death.

This elongation hypothesis is testable by: i), genetically engineering mice to overexpress PrP^C_{Tg}, which will quadratically modulate the PrP-res concentration (4), and ii), by varying the initial dose of PrP^{Sc}, which will linearly modulate the PrP-res concentration.

doi: 10.1529/biophysj.106.081703

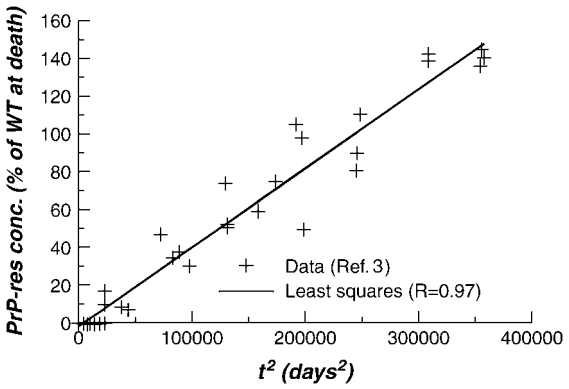

FIGURE 1 Quadratic-in-time fit to infectious prion time course data of Chesebro et al. (3).

Another striking observation of Chesebro et al. (3) was that mice heterozygous for expression of PrP^{C}_{Tg} and PrP^{C}_{WT} display shorter incubation time upon inoculation than mice with one PrP^{C}_{WT} copy and one inactive fusion construct. We argue that this is due to an enhanced concentration for PrP^{C}_{Tg} relative to PrP^{C}_{WT} and that PrP-res obtained from PrP^{C}_{Tg} also templates PrP^{C}_{WT} conversion. The latter is speculative but should be testable.

To establish the expectation that the PrP^{C}_{WT} concentration is lower than PrP^{C}_{Tg} in the WT/Tg heterozygotes, it is sufficient to establish that PrP^{C}_{WT} concentration in WT mice is lower than PrP^{C}_{Tg} concentration in the anchorless Tg mice. To make this clear, we compare estimates for cellular prion concentrations in homozygous WT mice with homozygous Tg mice. Before the postulated cell-death driven saturation of infectious material, WT mice inoculated with a concentration $[PrP^{Sc}_{n}]$ of scrapies seeds will have a time course of the general form (4)

$$[\text{PrP-res}](t) \propto A_{+}(\cosh[\lambda t] - 1), \tag{2}$$

where $\lambda = \ln(2)/t_2$ is the percentage growth rate and t_2 is the doubling time. The coefficient A_+ can be determined from

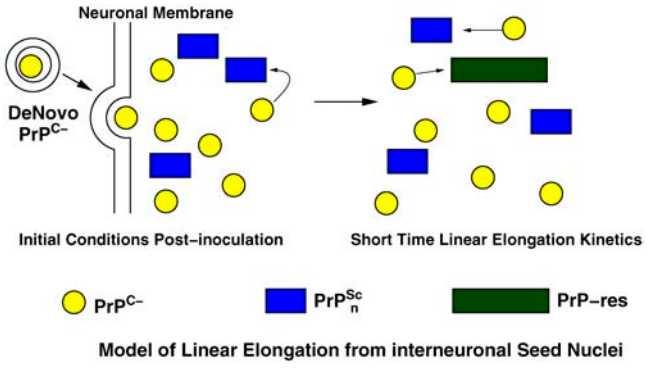

FIGURE 2 Schematic model for linear elongation driven growth of infectious prion material from inoculated seeds and anchorless cellular prion proteins.

the short time behavior of Eq. 2, which, like Eq. 1, is described by linear elongation given by

$$1/2\,A_{+}(\lambda t)^2 = 1/2\,(p_{+}[PrP^{C}_{WT}])^2[PrP^{Sc}_{n}]t^2, \tag{3}$$

where $[PrP^{C}_{WT}]$ is the homeostatic concentration of membrane bound WT PrP^{C} and we have assumed that the WT and Tg mice have the same PrP-res elongation coefficient p_+.

On the other hand, at long times (but before saturation) Eq. 2 gives

$$[\text{PrP-res}](t) \propto 1/2\,A_{+}\exp(\lambda t). \tag{4}$$

Now, we set $t_+ = N_d^+ t_2$ as the time it takes WT mice to reach clinically detectable levels of PrP-res concentration at the inoculum level generating a seed nuclei concentration $[PrP^{Sc}_{n}]$, where N_d^+ is the number of doublings experienced in that process, and t_- is the time it takes Tg mice to reach the same clinical concentration of PrP-res for the same initial inoculation dose. By taking suitable ratios to eliminate A_+, $[PrP^{Sc}_{n}]$, and p_+, the ratio of homeostatic concentrations of cellular prions from the WT mice to the Tg mice is given by

$$[PrP^{C}_{WT}]/[PrP^{C}_{Tg}] = (1/2)\ln(2)\,N_d^+\,(t_-/t_+) \times \exp(-\ln(2)(N_d^+/2)). \tag{5}$$

From Chesebro et al. (3), $t_+ = 150$ days, and $t_- = 400$ days. A reasonable estimate (5) for the number of doublings is $N_d^+ = 20$ for the dose of Chien et al. (1). With these numbers, Eq. 5 gives a concentration ratio (and hence elongation rate ratio) for WT/Tg mice of 0.036. This is reasonable given that likely slower PrP^{C} clearance in the Tg case will lead to a higher extracellular concentration of cellular prion protein. By employing the arguments of Chien et al. (1) we obtain elongation rate values of 0.13/day(Wt) and 3.5/day (Tg). The former is in good agreement with estimates made elsewhere for linear elongation based upon analysis of dose-incubation curves (6).

Hence, in the WT/Tg and WT/null heterozygotes explored in Chesebro et al. (3), we anticipate in each case the membrane bound PrP^{C}_{WT} concentration to be about half that of the homozygous WT mice, whereas the intercellular PrP^{C}_{Tg} concentration should be about half that of the homozygous Tg mice. Because, as shown with infectious prions bound to electrodes (7), templating and conversion can be driven by scrapies material not bound to the membrane surface, we expect the incubation time of the WT/Tg heterozygotes to be significantly accelerated relative to the WT/null heterozygotes as is observed.

We note that membrane associated exponential growth might be due to: i), as yet undiscovered membrane specific enzymes splitting aggregates, in analogy to the role of Hp104a for yeast prions (1); ii), mechanical breakage of aggregates due to membrane curvature or membrane undulations (8); iii), oligomeric autocatalysis arising from interneuronal

templating by infectious oligomeric seeds bound to one or the other membrane (9).

ACKNOWLEDGMENTS

We are grateful for conversations with H. Levine, J. N. Onuchic, M. Oldstone, A. N. Parikh, and J. Weissman.

We acknowledge the support of the U.S. Army (Congressionally Directed Medical Research Program, grant NP020132) (D.L.C. and R.P.P.S), National Science Foundation grant PHY0216576 (D.L.C. and S.Y.), and the J. S. Guggenheim Memorial Foundation (D.L.C.).

REFERENCES and FOOTNOTES

1. Chien, P., J. S. Weissman, and A. H. DePace. 2004. Emerging principles of conformation based prion inheritance. *Annu. Rev. Biochem.* 73: 617–656.
2. Collins, S. R., A. Douglass, R. Vale, and J. S. Weissman. 2004. Mechanism of prion propagation: amyloid growth occurs by monomer addition. *PLoS Biol.* 2:10–18.
3. Chesebro, B., M. Trifilo, R. Race, K. Meade-White, C. Teng, R. LaCasse, L. Raymond, C. Favara, G. Baron, S. Priola, B. Caughey, E. Masliah, and M. Oldstone. 2005. Anchorless prion protein results in infectious amyloid disease without clinical scrapie. *Science*. 308:1435–1439.
4. Ferrone, F. A. 1999. Analysis of protein aggregation kinetics. *Methods Enzymol.* 309:256–274.
5. Carlson, G. A., C. Ebeling, S. L. Yang, G. Telling, M. Torchia, D. Groth, D. Westaway, S. J. DeArmond, and S. B. Prusiner. 1994. Prion isolate specified allotypic interactions between the cellular and scrapie prion proteins in congenic and transgenic mice. *Proc. Natl. Acad. Sci. USA*. 91:5690–5694.
6. Kulkarni, R. V., A. Slepoy, R. R. P. Singh, D. L. Cox, and F. Pazmandi. 2003. 2003. Theoretical modeling of prion disease incubation. *Biophys. J*. 85:707–718.
7. Flechsig, E., I. Hegyi, M. Enari, P. Schwarz, J. Collinge, and C. Weissmann. 2001. Transmission of scrapie by steel-surface-bound prions. *Mol. Med*. 7:679–684.
8. Slepoy, A., R. R. P. Singh, F. Pazmandi, R. V. Kulkarni, and D. L. Cox. 2001. Statistical mechanics of prion disease. *Phys. Rev. Lett*. 87:058101.
9. Yang, S. C., H. Levine, J. N. Onuchic, and D. L. Cox. 2005. Structure of infectious prions: stabilization by domain swapping. *FASEB J*. 19: 1778–1782.

www.mrs.org/publications/bulletin

The Materials Science of Protein Aggregation

D.L. Cox, H. Lashuel, K.Y. C. Lee, and R.R.P. Singh

Abstract

Numerous human diseases are associated with conformational change and aggregation of proteins, including Alzheimer's, Parkinson's, prion diseases (such as mad cow disease), familial amyotrophic lateral sclerosis (ALS, or Lou Gehrig's disease), Huntington's, and type II (mature onset) diabetes. In many cases, it has been demonstrated that conformational change and aggregation can occur outside living cells and complex biochemical networks. Hence, approaches from materials and physical science have enhanced our understanding of the role of protein aggregation in these diseases at the molecular and nanoscale levels. In this article, we will review what is known about these protein structures from the perspective of materials science, focusing on the details of emergent oligomeric and nanotube-like structures, their interactions with model lipid bilayers, how the structures relate to observed biological phenomena, and how protein aggregation and amyloid formation can be employed for the good in biology and materials science.

Keywords: *amyloid diseases, complex adaptive matter, emergent behavior, prion diseases, protein aggregation, protofibrils, nanotubes, nanowires.*

Amyloid Diseases: A Truly Emergent Phenomenon

The primary goal of the study of complex adaptive matter is to identify the key organizing principles that govern materials phenomena at given length and time scales. In the case of the folding of individual globular proteins into their functional structures, we know a great deal. For example, the local rules governing α-helical secondary structure have been understood in detail for some 40 years;[1,2] indeed, the α-helix was predicted by Pauling and collaborators prior to discovery.[3] For the global tertiary structure of the protein, extensive experiments and simulation studies show that proteins engineered by evolution to experience minimal frustration in the interactions between closely contacted amino acids (or residues) develop funneled energy landscapes and relatively rapid (and multiple) pathways to folding after synthesis.[4] As discussed in the article by Ramirez in this issue, "frustration" refers to the effect of competing interactions that make it impossible to favorably lower the interaction energy.

However, we have comparatively little understanding of the organizing principles governing structure formation for proteins interacting with other proteins or membranes. This lack of knowledge is problematic, because proteins left alone tend to spontaneously aggregate, often by formation of β-sheet structures, which are not governed by local formation rules like α-helices (the distances between hydrogen bonding residues along the backbone can be great). β-sheets are formed from approximately linear stretches of peptide that hydrogen-bond from line to line. These structures are especially prone to protein aggregation due to favorable edge-to-edge hydrogen bonding between sheets.[5] This aggregation tendency is an obstacle in high-throughput proteomics, where one is interested in measuring the properties of individual proteins.[6]

Purposeful biological aggregation of monomeric proteins, as in the assembly of actin filaments or microtubules,[7] is usually highly regulated and energetically controlled (we will discuss tightly controlled and biologically useful β-sheet self-assembly later in the article). Living organisms have evolved an effective quality-control system to prevent protein misfolding and aggregation, where chaperone proteins provide "safe houses" for folding proteins,[8] and the ubiquitin/proteosome system ensures rapid degradation or disposal of misfolded proteins.

Table I conveys the tragic side of uncontrolled β-sheet self-assembly: it summarizes the key aspects of seven (out of dozens) prominent human amyloid diseases. Amyloid means "starch-like"—the aggregates stain like starch. These diseases typically arise in old- or middle-aged populations, and frequently arise spontaneously or sporadically rather than from genetic predisposition. Indeed, for spontaneous Alzheimer's, Parkinson's, prion, and immunoglobulin light chain diseases, incidence varies little between countries. Moreover, prion diseases, the lone infectious type of amyloid disease, show highly reproducible dose-versus-incubation-time distributions for intercerebrally inoculated animals.[9] Remarkably, infectious protein-only prion aggregates have been grown *in vitro*,[10] proving that the protein interaction properties alone, without additional biochemical guidance, account for the disease.

These observations suggest that these diseases can be studied from the perspective of materials growth, without extensive biological modulation. Indeed, it appears that the growth of amyloid structure has much in common with the oriented aggregation of inorganic, nearly monodispersed nanoparticles.[11] We seek here to portray the growing scientific movement toward the use of concepts and tools from materials science in the study of amyloidogenic proteins to elucidate the mechanisms of disease and design new materials.

Amyloid Structures: Plaques, Protein Nanotubes, and Oligomers

Plaques

The extracellular and/or intracellular accumulation of amyloid fibrils in the form of plaques or inclusions (Lewy bodies) in the brain is a defining hallmark for several neurodegenerative diseases (Figure 1). For example, Alzheimer's disease patients have large quantities of postmortem brain plaques, predominantly composed of 40–42-amino-acid-long Aβ peptides that are cleaved by protease proteins from the Alzheimer's precursor protein (BAPP).[13] These micrometer-scale plaques are composed of multi-polymeric strands of the peptide, called fibrils (Figure 1e), which

Table I: Aspects of Some Human Amyloid Diseases with Associated Protein Aggregation.

Disease	Protein/Peptide	Function	Heritable Component	Incidence	Onset Age* (Years)
Alzheimer's[51]	β-42 (from BAPP) and τ	?	~25%	~50% of post-85-yr-old population	>65
Parkinson's[52]	α-synuclein	?	5–10%	~1% of post-50-yr-old population	55–60 yrs
Huntington's[23]	huntingtin	?	100%	1 in 20,000 (Caucasian)	35–40
Familial ALS (Lou Gehrig's disease)[53]	Superoxide dismutase (20% of cases)	Lowers oxidative stress	100% (5–10% of all ALS)	2 in 10^6	46
Type II diabetes[54]	IAPP	?	High (obesity trigger)	14×10^6 per year (U.S.)	>40
Immunoglobulin light chain[55]	IG light chain	Immune response	Small/unknown	1 in 10^5	64
Prion diseases[35]	PrP^c	Lowers oxidative stress?	10–15%	~1 in 10^6	63

*Incidence/onset age is for non-heritable sporadic disease, unless otherwise noted.

have high quantities of β-sheet structure as revealed by crystallography, circular dichroism (which detects the different light polarization rotation tendencies of α-helices and β-sheets), and more recently, solid-state magnetic resonance studies. These β-strands are aligned perpendicular to the fibrillar axis, in a so-called "cross-β" structure, shown in Figure 1f. Postmortem plaques and inclusions from a variety of diseases are shown in Figure 1.[13] We note that the amyloid fibrils are protein nanotubes, hollow in the middle, with diameters of the order of 10–20 nm.

Despite a dominant research focus on both structure measurements and computer modeling on plaques, an emerging perspective is that the plaques may represent disease end points having little to do with toxicity.[14] This view is supported by observations such as (1) the abundant Aβ plaques observed in the brains of individuals displaying no symptoms of Alzheimer's disease and (2) the non-uniformity of plaque observation in prion diseases: for example, victims of kuru (a disease among the Fore people of New Guinea, arising from ritual cannibalism of deceased tribe members) exhibit them, while victims of spontaneous Creutzfeldt-Jakob disease usually do not.[15] In this view, toxicity is engendered by small β-sheet aggregates, possibly on the pathway to amyloid fibrils.

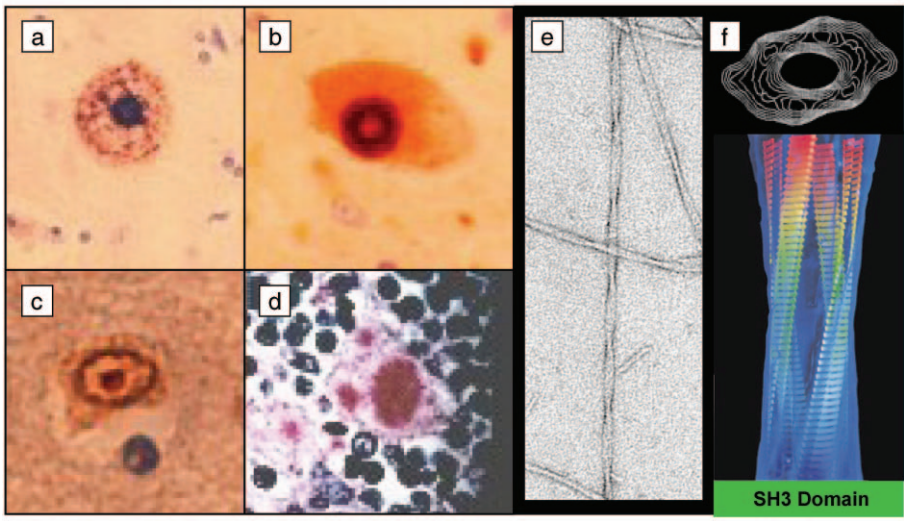

Figure 1. Plaques and fibrils. (a)–(d) Postmortem tissue plaques from human amyloid disease patients (from Reference 13): (a) Aβ42 (Alzheimer's) plaque, (b) α-synuclein (Parkinson's) plaque, (c) huntingtin plaque (Huntington's disease), and (d) PrP^{Sc} (kuru) plaque. (e) Transmission electron microscope images of amyloid fibrils (H. Lashuel, unpublished data). (f) Model of a hollow-core SH3 domain fibril: upper panel shows a density map cross section, lower panel shows the cross-β structure.[56]

β-Helices

Accordingly, attention has turned to small β-sheet motifs with multiple assembly outcomes, especially the left-handed β-helix (LHBH) structures shown in Figure 2,[16] recently proposed as the β-sheet unit for infectious mammalian prion trimers on the basis of cryogenic electron microscopic data.[17] The LHBH β-sheet structure has also been proposed for yeast prion-like proteins,[18] Alzheimer's disease,[19] and Huntington's disease.[16,20] This LHBH motif was first observed in several bacterial enzymes and the "antifreeze" protein of the spruce budworm; to date, there are 11 structures in the protein data bank (http://www.rcsb.org/pdb/) confirmed to have LHBHs. LHBHs are usually presumed (or, in two cases, observed)[21,22] to be in protein trimers. The LHBH motif has a fundamental repeat unit of triangular cross section, consisting of 18 amino acids with two per bend region and four per

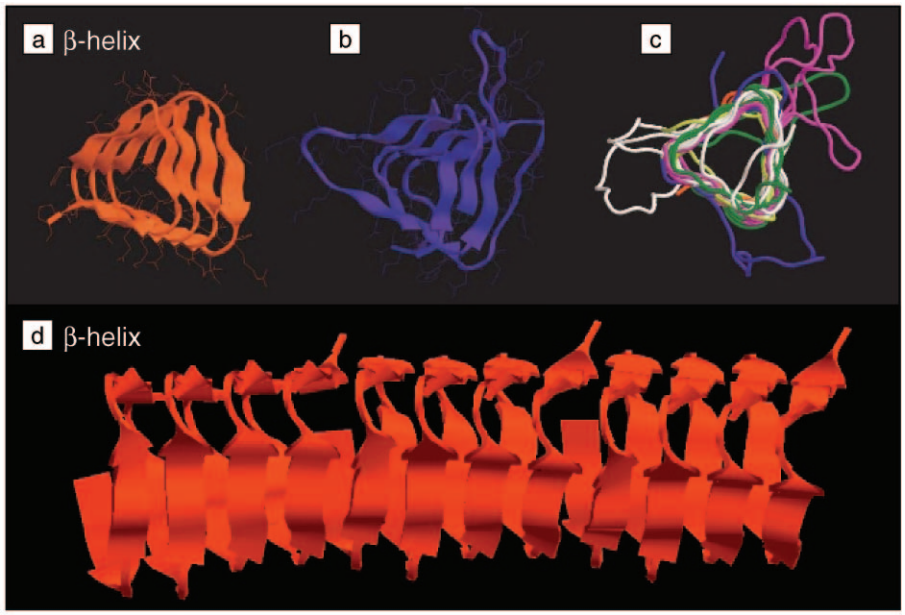

Figure 2. (a) Peptide backbone of measured left-handed β-helix (LHBH) structure of 1FWY protein. (b) Proposed LHBH structure of infectious prion protein (after Reference 16). Parallel, hydrogen-bonded β-sheets are shown as strips. (c) Superposed structure of six LHBH backbones, illustrating the uniform cross section of the helical structure (red, 1FWY protein; blue, proposed infectious prion protein; yellow, 1HMO protein; white, 1J2Z protein; green, 1L0S protein; fuchsia, 1T3D protein). (d) LHBH "nanotube" formed from a stack of three 1FWY helices. All images generated with the RASTOP molecular viewing program (see www.geneinfinity.org/rastop/); all files for the proteins 1FWY, 1HMO, 1J2Z, 1L0S, and 1T3D input to RASTOP are from the Protein Data Bank (http://www.rcsb.org), except for the PrP^{Sc} model, which is courtesy of C. Govaerts.

β-strand, alternating between hydrophobic and hydrophilic in the strand. The triangular cross section is very uniform across observed LHBHs (Figure 2c); each edge is ~1.9 nm in length. In Figure 2d, we show how multiple copies of the LHBH of an enzyme from *E. coli* (labeled 1FWY on the protein data base at www.rcsb.org/pdb) can be assembled into a kind of β-nanotube. This raises the natural and intriguing question: are amyloid fibrils composed of such "nanofilaments"?[19]

The LHBH has a tantalizing connection to Huntington's and other polyglutamine repeat diseases, where pathology derives from an inherited excess number of repeats of the amino acid glutamine on one end (the N-terminus) of the huntingtin protein.[23] A polyglutamine repeat number p of less than ~24 is normal; for $p > 36$, disease is certain. Note that 36 is the number of amino acids or residues in two turns of a LHBH that has fully saturated internal hydrogen bonds.[19]

The LHBH presents a challenge to theory and simulation. At present, this motif has not emerged from any molecular dynamics simulations or semi-analytic (Hamiltonian or cellular automata) approaches. The complicating factor is the long-range coupling along the backbone (bonded amino acids are separated by 18 residues). On the other hand, the remarkable conservation of the shape and helical cross section suggest that this is a motif ripe for study.

Nanoscale Oligomers

β-sheet oligomers obtained from *in vitro* growth of aggregates have been studied extensively.[13] One common form seems to be a spherical micelle-like aggregate of β-converted proteins, which have been implicated as precursors for the chain-like (protofibril) and annular oligomers that are also seen frequently during *in vitro* amyloid formation by most amyloidogenic proteins.[24] Figure 3 shows a compendium of oligomers and protofibrils from amyloid disease proteins.[25,26] The annular oligomers underlie the proposed toxicity mechanism discussed later in this article. We note that all atomic force microscope (AFM) measurements of spherical, chain-like, and annular oligomers share the same height and diameter, suggesting that the spherical aggregates are the precursors to the larger chain and annular pore-like structures.

The diversity of pre-fibrillar oligomer structures, the formation of which are highly dependent upon protein sequence and environmental conditions (e.g., pH, salt concentration, and levels of molecular crowding), may explain the mystery of prion disease strains. Strains, for a given mammal, have unique incubation-time versus dose distributions, tissue lesion profiles, and distributions of post-translationally attached sugars: the prion protein can have 0, 1, or 2 sugars attached.[27,28] Moreover, strains breed true upon multiple passage in animals. This means that upon passage from a diseased animal to a healthy animal, the same properties (incubation time, lesion profile, sugar binding) are preserved. There is considerable evidence that strain is encoded in prion conformation but no detailed understanding of the underlying mechanisms.[27,28] Prion oligomers[17] might have a spectrum of different shapes, and oriented aggregation of such protein "nanoparticles" might "breed" the conformation true (nonmatching shapes will be energetically unfavorable).

Domain Swapping

A separate way to generate fibrils and oligomers is by "domain swapping,"[29,30] in which, say, two identical copies (A,B) of a protein exchange a domain (a well-defined protein region attached to a flexible section of peptide). The domain of monomer A binds to the corresponding region of B and vice versa. The swapping is not limited to dimers; it can lead to filamentary structures in which the ith protein swaps with the $(i + 1)$th protein, for example, closed-chain oligomers (where filament ends are brought together to domain-swap) or two-dimensional structures.

Domain swapping has been proposed to play a role in prion strains.[31] Domain swapping in protein–protein interactions generically and amyloid diseases in particular seems certain to emerge as a critical theme in the coming years. At the conceptual level, the study of coarse-grained protein models with molecular dynamics has shown that the formation of domain-swapped dimers will proceed down a funneled landscape if the dimer enjoys minimal frustration.

Aggregation Pathways and Kinetics

AFM and kinetic modeling, well known to materials scientists, have been instrumental in advancing our understanding of the structural properties of the protein aggregates linked to disease and their growth kinetics. Figure 4 schematically shows accepted models on amyloid conversion/aggregation kinetics. We note

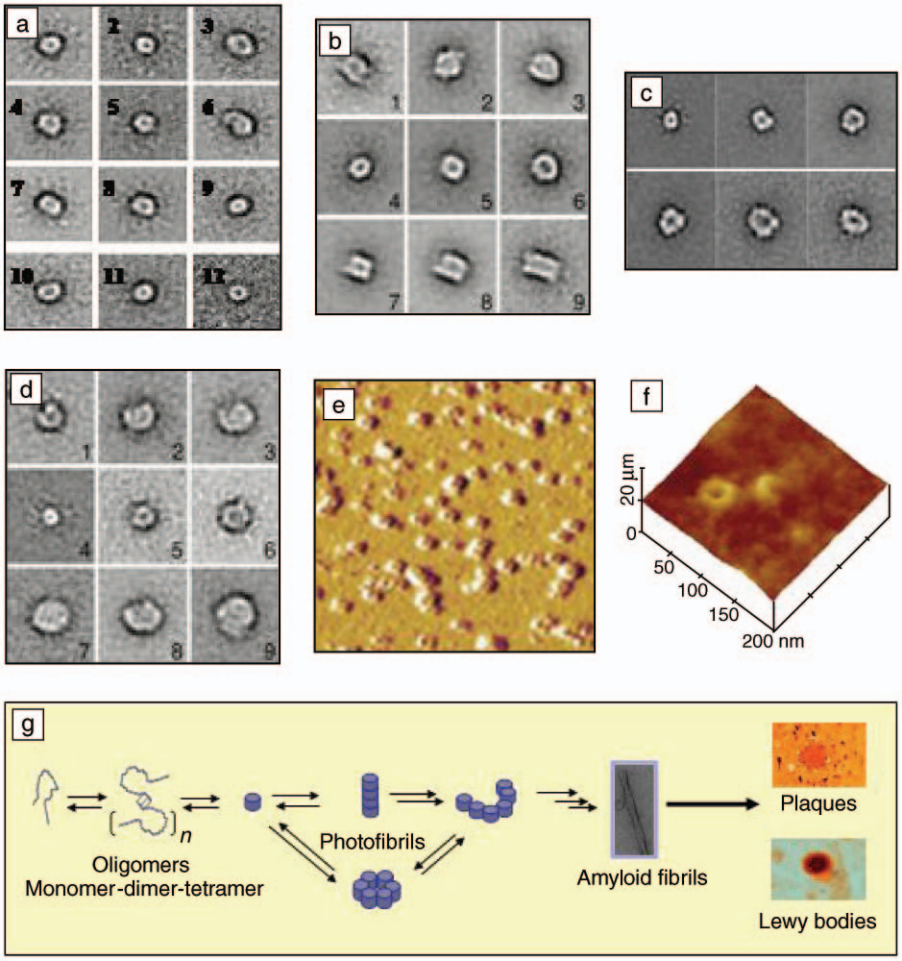

Figure 3. Amyloid oligomers. (a) Aβ peptide implicated in Alzheimer's disease, observed by electron microscopy (scale, 50 nm/box) (from Reference 24). (b) Nine different oligomers of mutant α-synuclein, implicated in Parkinson's disease, observed by electron microscopy (scale, 40.5 nm/box) (from Reference 25). (c) Six oligomers of mutant SOD1, implicated in familial ALS (from Reference 56).[57] (d) Nine mutant α-synuclein oligomers (scale, 40.5 nm/box) (from Reference 25). (e) Atomic force microscope (AFM) images of Aβ oligomers inserted in a supported lipid bilayer (from Reference 26). Clearly resolved annular oligomers have outer diameters of ~16 nm. (f) AFM image of α-synuclein oligomer on supported lipid bilayer (from Reference 25). (g) Schematic illustration of oligomerization pathways. Here, the subscript n *in the second stage represents the number of monomers in an oligomer.*

that β-sheet conversion is typically concomitant with aggregation (i.e., conformational changes and protein assembly are linked),[32,33] with the possible exception of polyglutamine proteins,[34] and requires templating either by spontaneously formed (and rare) nuclei or by external seeding of aggregates.[33] Also, fission of mammalian prions is necessary for disease propagation and exponentially growing aggregates in mammals; prion-like proteins in yeast have fission effected by another protein[35] (although the fission can occur spontaneously *in vitro*).[36] Why mammalian prions fission and other amyloidogenic proteins do not remains a mystery.

In vitro and theoretical studies of conversion/aggregation suggest that the late-age onset in amyloid diseases derives from slow underlying molecular processes. For example, *in vitro* kinetics experiments for polyglutamine peptides extrapolated to *in vivo* concentrations of huntingtin protein suggest that within the "sampling window" of a human lifespan, toxic aggregate concentrations should arise only for glutamine number $p > 36$, consistent with clinical observations.[34]

For prion diseases, theoretical modeling of two-dimensional aggregation and fission (prions live mostly on neuronal membranes) yielded a sporadic incubation time distribution that peaked at ~100 times that obtained from dilute seeding for physiological concentrations of the normally expressed protein called PrP^c that misfolds in the diseased form.[37] Given a mean incubation time for kuru of 12 years,[38] this suggests that endemic sporadic prion disease requires ~1000-year life spans! Meanwhile, the 1 in 10^6 sporadic disease background incidence may reflect the low-amplitude, pre-peak tail in the incubation time distribution.[38]

Amyloid–Membrane Interaction and Toxicity

Many amyloidogenic proteins associate with lipid membranes. AFM studies on supported bilayers and molecular modeling have helped support a potential unifying hypothesis for amyloid disease toxicity: that small oligomers pierce cell membranes, triggering cell death through superfluous ion pores. It was proposed in detail that a pair of β-coupled annular tetramers of Aβ peptides can insert into the neuronal membrane leaflets and create an ion pore.[39] *In vitro*-grown oligomers qualitatively consistent with this hypothesis have been found (Figure 3) and studied with AFM on supported bilayers (Figure 3f); these are evidently composed of 4 nm spherical oligomers, much larger than the peptide tetramers of Reference 39. These oligomers permit excess calcium flux, which is toxic to cultured neurons.[26] Intracerebral inoculation of rats and mice with a solution presumed rich in oligomeric Aβ particles leads to a reversible short-term memory deficit.[40] A recent theoretical study found strong correlations between the membrane insertion configuration and the pore model for 4 of 5 mutations leading to early-onset Alzheimer's disease.[41] While the pore model is not universally accepted, and may not apply to all the diseases (the prion trimer model, for example, will not allow ion passage), it remains a vibrant area of research.

Amyloids for Good in Biology and Materials Science

Biologically Useful Amyloids

Emerging evidence suggests that amyloid structures can provide useful biological functions. Some examples are

1. *Heritable amyloid structure in yeast.* As alluded to previously, prion-like proteins in yeast form aggregates that fission upon cell division, can actively confer phenotype, and may provide some stress protection.[42]
2. *Spider silk.* Spiders produce insoluble filaments of fibroin protein that possess 30× greater extensibility and toughness than steel. Recent circular dichroism studies show that significant amyloid-like cross-β structure develops in a region of reduced

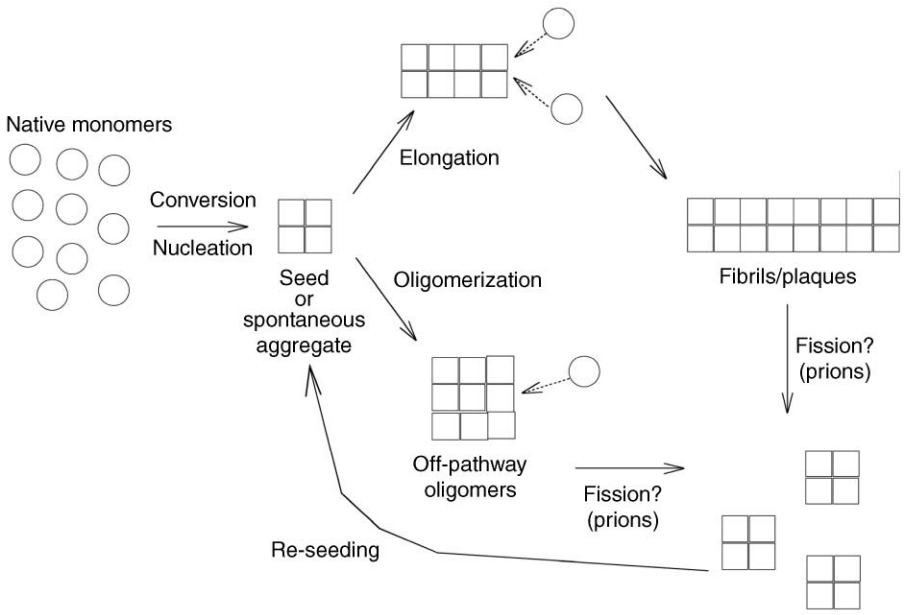

Figure 4. Schematic illustration of amyloid conversion and aggregation. Native monomers of the relevant peptides or proteins are shown as circles and high-β-content converted proteins as squares. Peptides can either spontaneously convert or be seeded. Subsequent aggregation and conversion can generate either proto-fibrils via the elongation step, which then form amyloid fibrils and plaques, or pass to "off-pathway" oligomers. In the case of prions, the oligomers and/or fibrils can fission, which then re-seeds the initial conversion/aggregation process. Prions are the only known amyloid proteins to spontaneously fission in the converted form either in vitro *or* in vivo*. It is assumed (but not shown explicitly here) that both oligomers and native monomers experience some level of removal by cellular systems* in vivo*.*

pH downstream from the initial extrusion site.[43]

3. *Chorion in fish and insect egg shells.* Truncated peptides from the central regions of two chorion proteins self-assembled into spherulites possessing β-structure, which then converted to fibrils upon maturation, suggesting amyloid character in actual egg shells.[44]

4. *Amyloid-like structure in synapses of Aplysia (slugs).* The N-terminus region of the *Aplysia* synapse protein CPEB is glutamine-rich, like huntingtin protein. Engineered expression of CPEB in yeast yields prion-like aggregates similar to the native ones discussed earlier; hence, prion-like states of CPEB might effect long-term strengthening of synaptic contacts.[45]

Amyloids in Materials Science

The regular diameter and periodicity of the amyloid fibrils make them good materials templates. One group employed yeast prion-like proteins to template ~100-nm-wide gold nanowire growth; the gold-coated protein filaments after initial decoration by small gold nanoparticles were found to bind to genetically engineered cysteine residues.[46] Silver nanowires of 20 nm width were grown *inside* filamentary cross-β tubes grown from a diphenylalanine peptide.[47] Engineering of controllably switched β-sheet materials could prove valuable for tissue growth scaffolding, as one example.[48] Hybrid molecules including eight amino acids—four per strand, but with non-amino bends—have been developed that controllably self-assemble into different β-sheet structures (as shown in Figure 5) depending upon the pH, analogous to spider silk.[49] Clearly, the future of engineered amyloid structures in materials science looks bright.[50]

Conclusion

In this article, we have developed themes that bring together the fields of amyloid diseases and materials science. Protein misfolding and aggregation phenomena are intimately linked to many serious public health issues. However, many aspects of the phenomena have close analogies in synthesized materials, and their full molecular understanding requires experimental and modeling tools more familiar in the physical and materials sciences. In addition to the possible medical breakthroughs that such multidisciplinary studies can lead to, there is a growing possibility that understanding the mechanisms of amyloid formation can have wide impact in fields ranging from basic neurobiology to materials science.

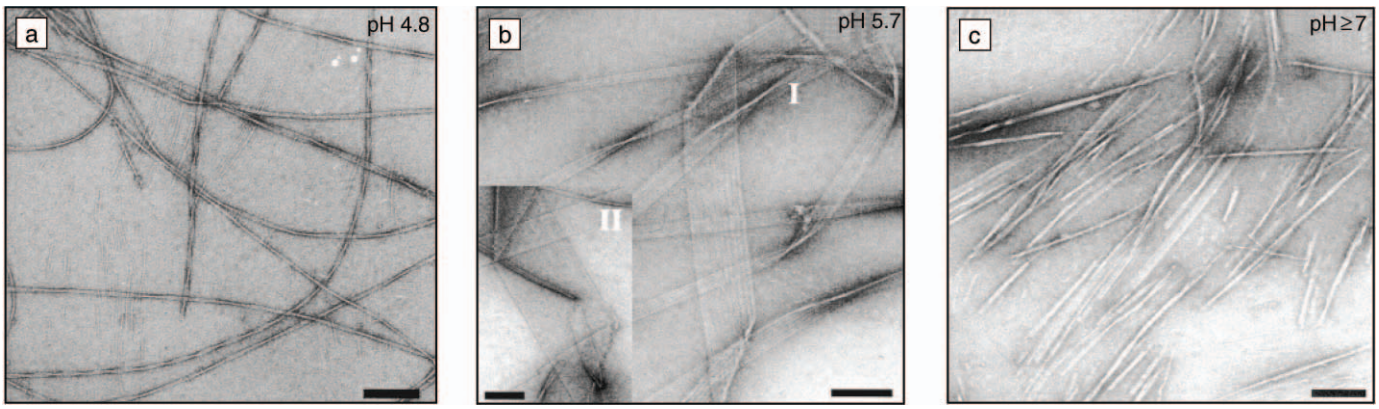

Figure 5. (a)–(c) Images from electron microscopy showing pH-dependent fibril growth of designed peptidomimetic molecules (from Reference 49). Scale bars are 100 nm.

Acknowledgments

D.L. Cox and R.R.P. Singh acknowledge the support of the U.S. Army Congressionally Directed Medical Research Fund, grant NP02013. D.L. Cox thanks the NSF Center for Theoretical Biological Physics, grant PHY 0120999, and S. Yang, H. Levine, and J. Onuchic for many useful discussions. We thank C. Govaerts for sharing the coordinates of the model prion trimer and R. Lal for sharing the second paper in Reference 26 prior to publication. This article is reflective of scientific discussions and presentations from two workshops on the physical properties of amyloids sponsored by the Institute for Complex Adaptive Matter (San Francisco, November/December 2001; Boston, February 2004).

References

1. B.H. Zimm and J.K. Bragg, *J. Chem. Phys.* **31 (**1958) p. 526.
2. S. Lifson and A.J. Roig, *J. Chem. Phys.* **34 (**1961) p. 1963.
3. L. Pauling, R.B. Corey, and H.R. Branson, *Proc. Natl. Acad. Sci. USA* **37** (1951) p. 205.
4. P.G. Wolynes, J.N. Onuchic, and D. Thirumalai, *Science* **267** (1995) p. 1619; J.N. Onuchic and P.G. Wolynes, *Curr. Opin. Struct. Biol.* **14** (2004) p. 70.
5. M. Stefani and C.M. Dobson, *J. Mol. Med.* **81** (2003) p. 678.
6. P.S. Lee and K.H. Lee, *Biotech. Bioeng.* **89** (2004) p. 195.
7. J.E. Bear, M. Krause, and F.B. Gertler, *Curr. Opin. Cell. Biol.* **13** (2001) p. 158; S. Inouye, *J. Struct. Biol.* **118** (1997) p. 87.
8. P.L. Clark, *Trends Biochem. Sci.* **29** (2004) p. 527.
9. S.B. Prusiner, J. Safar, and S.J. DeArmond, in *Prion Biology and Diseases* (Cold Spring Harbor Laboratory Press, Cold Spring Harbor, NY, 2004) p. 143.
10. G. Legname, I.V. Baskakov, H.-O.B. Nguyen, D. Riesner, F.E. Cohen, S.J. DeArmond, S.B. Prusiner, *Science* **306** (2004) p. 673.
11. R.L. Penn, *J. Phys. Chem. B* **108** (2004) p. 12707.
12. P.H. St. George-Hyslop, *Sci. Am.* **283** (2000) p. 76.
13. All plaque/inclusion images are from the laboratory of M. Feany, http://feany-lab.bwh.harvard.edu/link2/ (accessed April 2005).
14. B. Caughey and P.T. Lansbury Jr., *Annu. Rev. Neurosci.* **26** (2003) p. 267.
15. S. J. deArmond, J.W. Ironside, E. Bouzamondo-Bernstein, D. Peretz, and J.R. Fraser, in *Prion Biology and Diseases* (Cold Spring Harbor Laboratory Press, Cold Spring Harbor, NY, 2004) p. 777.
16. J. Jenkins and R. Pickersgill, *Prog. Biophys. Mol. Biol.* **77** (2001) p. 111.
17. C. Govaerts, H. Wille, S.B. Prusiner, and F.E. Cohen, *Proc. Nat. Acad. Sci. USA* **101** (2004) p. 8342.
18. A. Kishimoto, K. Hasegawa, H. Suzuki, H. Taguchi, K. Namba, and M. Yoshida, *Biochem. Biophys. Res. Commun.* **315** (2004) p. 739.
19. J.-T. Guo, R. Wetzel, and Y. Xu, *Proteins: Struct. Funct. Bioinformatics* **57** (2004) p. 357.
20. M.F. Perutz, J.T. Finch, J. Berriman, and A. Lesk, *Proc. Natl. Acad. Sci. USA* **99** (2002) p. 5591; R. Wetzel, *Structure* **10** (2002) p. 1031.
21. V.E. Pye, A.P. Tingey, R.L. Robson, and P.C.E. Moody, *J. Biol. Chem.* **279** (2004) p. 40729.
22. C. Kisker, H. Schindelin, B.E. Alber, J.G. Ferry, and D.C. Rees, *EMBO J.* **15** (1996) p. 2323.
23. H.Y. Zoghbi and H.T. Orr, *Annu. Rev. Neurosci.* **23** (2000) p. 217.
24. H.A. Lashuel, D.M. Hartley, B.M. Petre, J.S. Wall, M.N. Simon, T. Walz, and P.T. Lansbury, *J. Mol. Biol.* **332** (2003) p. 795.
25. H.A. Lashuel, B.M. Petre, J. Wall, M. Simon, R.J. Nowak, T. Walz, P.T. Lansbury, *J. Mol. Biol.* **322** (2002) p. 1089.
26. A. Parbhu, H. Lin, J. Thimm, and R. Lal, *Peptides* **23** (2002) p. 1265; A. Quist, I. Doudevski, H. Lin, R. Azimova, D. Ng, B. Frangione, B. Kagan, J. Ghiso, and R. Lal, et al., preprint submitted to *Nat. Struct. Biol.* (2005).
27. S.B. Prusiner, M.R. Scott, S.J. DeArmond, and G. Carlson, in *Prion Biology and Diseases* (Cold Spring Harbor Laboratory Press, Cold Spring Harbor, NY, 2004) p. 187.
28. M. Scott, D. Peretz, R.M. Ridley, H.F. Baker, S.J. DeArmond, and S.B. Prusiner., in *Prion Biology and Diseases,* Cold Spring Harbor Laboratory Press, Cold Spring Harbor, NY (2004) p. 435.
29. M.J. Bennett, M.P. Schlunegger, and D. Eisenberg, *Protein Sci.* **4** (1995) p. 2455; M.P. Schlunegger, M.J. Bennett, and D. Eisenberg, *Adv. Protein Chem.* **50** (1997) p. 61; Y. Liu, G. Gotte, M. Libonatti, and D. Eisenberg, *Nat. Struct. Biol.* **8** (2001) p. 211.
30. S.C. Yang, S.S. Cho, Y. Levy, M.S. Cheung, H. Levine, P.G. Wolynes, J.N. Onuchic, *Proc. Natl. Acad. Sci. USA* **101** (2004) p. 13786.
31. F.E. Cohen and S.B. Prusiner, *Annu. Rev. Biochem.* **67** (1998) p. 793.
32. T.R. Serio, A.G. Cashikar, A.S. Kowal, G.J. Sawicki, J.J. Moslehi, L. Serpell, M.F. Arnsdorf, and S.L. Lindquist, *Science* **289** (2000) p. 1317.
33. S. Chen, F.A. Ferrone, and R. Wetzel, *Proc. Natl. Acad. Sci. USA* **99** (2002) p. 11884.
34. J. Masel, V.A.A. Jansen, and M.A. Nowak, *Biophys. Chem.* **77** (1999) p. 139.
35. P. Chien, J.S. Weissman, and A.H. DePace, *Annu. Rev. Biochem.* **73** (2004) p. 617.
36. S.R. Collins, A. Douglass, R.D. Vale, and J.S. Weissman, *PLoS Biol.* **2** (2004) p. 1582.
37. A. Slepoy, R.R.P. Singh, F. Pazmandi, R.V. Kulkarni, and D.L. Cox, *Phys. Rev. Lett.* **87** 058101 (2001).
38. R.G. Will, M.P. Alpers, D. Dormont, and L.B. Schonberger, in *Prion Biology and Diseases* (Cold Spring Harbor Laboratory Press, Cold Spring Harbor, NY, 2004) p. 629.
39. N. Arispe, H. B. Pollard, and E. Rojas, *Proc. Natl. Acad. Sci. USA* **90** (1993) p. 10573; N. Arispe, H.B. Pollard, and E. Rojas, *Mol. Cellu. Biochem.* **140** (1994) p. 119; S.R. Durell et al., *Biophys. J.* **67** (1994) p. 2137.
40. D.M. Walsh, I. Klyubin, J.V. Fadeeva, W.K. Cullen, R. Anwyl, M.S. Wolfe, M.J. Rowan, and D.J. Selkoe, *Nature* **416** (2002) p. 535.
41. D.L. Mobley, D.L. Cox, R.R.P. Singh, M.W. Maddox, and M.L. Longo, *Biophys. J.* **86** (2004) p. 3585.
42. H.L. True, I. Berlin, and S.L. Lindquist, *Nature* **431** (2004) p. 184.
43. C. Dicko, F. Vollrath, and J.M. Kenney, *Biomacromolecules* **5** (2004) p. 704.
44. S.J. Hamodrakas, A. Hoenger, and V.A. Iconomidou, *J. Struct. Biol.* **145** (2004) p. 226.
45. K. Si, S. Lindquist, and E.R. Kandel, *Cell* **115** (2004) p. 879.
46. T. Scheibel, R. Parthasarathy, G. Sawicki, X.M. Lin, H. Jaeger, and S.L. Lindquist, *Proc. Natl. Acad. Sci. USA* **100** (2003) p. 4527.
47. M. Reches and E. Gazit, *Science* **300** (2003) p. 625.
48. C.E. MacPhee and D.N. Woolfson, *Curr. Opin. Solid State Mater. Sci.* **8** (2004) p. 141.
49. H.A. Lashuel, S.R. LaBrenz, L. Woo, L.C. Serpell, J.W. Kelly, *J. Am. Chem. Soc.* **122** (2000) p. 5262.
50. S.H. Waterhouse and J.A. Gerrard, *Aust. J. Chem.* **57** (2004) p. 519.
51. S. Gao, H.C. Hendrie, K.S. Hall, and S. Hui, *Arch. Gen. Psychiatry* **55** (1998) p. 809.
52. S.C. Conley and J.T. Kirchner, *Postgrad. Med. Online* **106** (1) (1999), http://www.postgradmed.com/issues/1999/07_99/conley.htm (accessed April 2005).
53. M.J. Strong, A.J. Hudson, and W.G. Alvord, *Can. J. Neurol. Sci.* **18** (1991) p. 45.
54. S.R. Votey and A.L. Peters, "Diabetes Mellitus, Type II—A Review," http://www.emedicine.com/emerg/topic134.htm (accessed April 2005).
55. R.H. Falk, R.L. Comenzo, and M. Skinner, *New Eng. J. Med.* **337** (1997) p. 898.
56. J.L. Jimenez, J.I. Guijarro, E. Orlova, J. Zurdo, C.M. Dobson, M. Sunde, H.R. Saibil, *EMBO J.* **18** (1999) p. 815.
57. S.S. Ray, R.J. Nowak, K. Strokovich, R.H. Brown, T. Walz, and P.T. Lansbury, *Biochem. U.S.* **43** (2004) p. 4899. □

APPENDIX G

News Results

NEWS STORIES Results **1 - 18** of about **18** for **Cox Singh "mad cow"**. Sort Results by:

1. California researcher finds that **mad cow** infection spreads rapidly
   Scottsbluff Star-Herald - Jun 16 8:06 AM
   DAVIS, Calif. (AP) - Researchers at the University of California, Davis are trying to explain how **mad cow** so frighteningly fast.

2. Modeling to Understand **Mad Cow** Disease
   SAP Info - Jun 16 2:15 AM
   Two physics professors at the University of California Davis, who have been researching **mad cow** disea use computerized mathematical models to explain how the disease acts so fast.

3. Researchers explore spread of **mad cow** disease
   CTV.ca - Jun 15 4:49 PM
   DAVIS, Calif. — Researchers at the University of California, Davis are trying to explain how **mad cow** dis frighteningly fast using an unconventional tool mathematical modeling.

4. UC Researchers Explore Spread of **Mad Cow**
   TechNewsWorld.com - Jun 15 8:27 AM
   Scientists believe the human body usually rejects misfolded proteins without harm; it's when a microscopi flawed proteins is consumed from another animal that the disease can take hold in a person or animal wh would never develop the disease.

5. The Capital City's Newspaper Online
   Independent Record - Jun 14 11:12 PM
   AP photo - Rajiv **Singh**, a physics professor at the University of California Davis, holds up a slide showing of a human protein cell at his campus office in Davis, Calif., on Tuesday.

6. **Mad cow** computer modeling finds infection spreads rapidly
   Billings Gazette - Jun 15 7:31 AM
   DAVIS, Calif. -- Researchers at the University of California, Davis are trying to explain how **mad cow** dise frighteningly fast using an unconventional tool -- mathematical modeling.

7. **Mad cow** computer modeling finds infection spreads rapidly
   Billings Gazette - Jun 15 7:32 AM
   DAVIS, Calif. -- Researchers at the University of California, Davis are trying to explain how **mad cow** dise frighteningly fast using an unconventional tool -- mathematical modeling.

8. UC Researchers Explore Spread of **Mad Cow**
   First Coast News - Jun 15 10:04 AM
   DAVIS, CA (AP) -- Researchers at the University of California, Davis are trying to explain how **mad cow** frighteningly fast using an unconventional tool - mathematical modeling.

9. **Mad cow** computer modeling finds infection spreads rapidly

SanLuisObispo.com - Jun 15 3:35 AM
DAVIS, Calif. - Researchers at the University of California, Davis are trying to explain how **mad cow** dise
frighteningly fast using an unconventional tool - mathematical modeling.

10. UC researchers explore spread of **mad cow**
Kansas City Star - Jun 15 5:20 AM
DAVIS, Calif. - Researchers at the University of California, Davis are trying to explain how **mad cow** dise
frighteningly fast using an unconventional tool - mathematical modeling.

11. UC Researchers Explore Spread of **Mad Cow**
RedNova - Jun 15 7:26 AM
DAVIS, Calif. -- Researchers at the University of California, Davis are trying to explain how **mad cow** dise
frighteningly fast using an unconventional tool - mathematical modeling.

12. UC researchers explore spread of **mad cow**
The Times Leader - Jun 15 5:18 AM
DAVIS, Calif. - Researchers at the University of California, Davis are trying to explain how **mad cow** dise
frighteningly fast using an unconventional tool - mathematical modeling.

13. UC researchers explore spread of **mad cow**
Macon Telegraph - Jun 15 5:28 AM
DAVIS, Calif. - Researchers at the University of California, Davis are trying to explain how **mad cow** dise
frighteningly fast using an unconventional tool - mathematical modeling.

14. **Mad cow** computer modeling finds infection spreads rapidly
Monterey County Herald - Jun 15 3:29 AM
DAVIS, Calif. - Researchers at the University of California, Davis are trying to explain how **mad cow** dise
frighteningly fast using an unconventional tool - mathematical modeling.

15. UC researchers explore spread of **mad cow**
TimesLeader.com - Jun 15 5:08 AM
DAVIS, Calif. - Researchers at the University of California, Davis are trying to explain how **mad cow** dise
frighteningly fast using an unconventional tool - mathematical modeling.

16. **Mad cow** computer modeling finds infection spreads rapidly
The Times Leader - Technology - Jun 15 5:48 AM
DAVIS, Calif. (AP) - Researchers at the University of California, Davis are trying to explain how **mad cow**
so frighteningly fast using an unconventional tool -- mathematical modeling.

17. UC Researchers Explore Spread of **Mad Cow**
WJLA-TV Washington D.C. - Jun 15 6:08 AM
DAVIS, Calif. (AP) - Researchers at the University of California, Davis are trying to explain how **mad cow**
(news) acts so frighteningly fast using an unconventional tool - mathematical modeling.

18. UC researchers explore spread of **mad cow**
Kansas City Star - Jun 15 5:27 AM
DAVIS, Calif. - Researchers at the University of California, Davis are trying to explain how **mad cow** dise
frighteningly fast using an unconventional tool - mathematical modeling.